Biomedicine & Pharmacotherapy 93 (2017) 1098–1115

Available online at
ScienceDirect
www.sciencedirect.com

Elsevier Masson France
EM|consulte
www.em-consulte.com/en

Review

Magnetic iron oxide nanoparticles as novel and efficient tools for atherosclerosis diagnosis

María Gabriela Montiel Schneider, Verónica Leticia Lassalle*

INQUISUR, Departamento de Química, Universidad Nacional del Sur (UNS)-CONICET, Av. Alem 1253, 8000 Bahía Blanca, Argentina

ARTICLE INFO

Article history:
Received 6 March 2017
Received in revised form 14 June 2017
Accepted 5 July 2017

Keywords:
Magnetic nanoparticles
Iron oxide
Atherosclerosis
Diagnosis
MRI

ABSTRACT

Cardiovascular complications derivate from atherosclerosis are the main cause of death in western world. An early detection of vulnerable atherosclerotic plaques is primordial for a better care of patients suffering the pathology. In this context nanotechnology has emerged as a promising tool to achieve this goal. Nanoparticles based on magnetic iron oxide (MNPs) have been extensively studied in cardiovascular diseases diagnosis, as well as in the treatment and diagnostic of other pathologies. The present review aims to describe and analyze the most current literature regarding to this topic, offering the level of detail required to reproduce the experimental tasks providing a critical input of the latest available reports. The current diagnostic features are presented and compared, highlighting their advantages and disadvantages. Information on novel technology intended to this purpose is also recompiled and in deep analyzed. Special emphasis is placed in magnetic nanotechnology, remarking the possibility to assess selective and multifunctional systems to the early detection of artherosclerotic pathologies.

Finally, in view of the state of the art, the future perspectives about the trends on MNPs in artherosclerorsis diagnostic and treatment have also been addressed.

Contents

1. Introduction . . . 1098
2. General aspects of imaging diagnosis, differences between them . . . 1099
3. Magnetic iron oxide nanoparticles . . . 1100
   3.1. General aspects of MNPs in diagnosis . . . 1100
      3.1.1. MNPs in the market . . . 1101
   3.2. Principal techniques to prepare MNPs for biomedical applications . . . 1102
   3.3. Different coating and strategies to assess stable MNPs in dispersion . . . 1103
4. Magnetic nanoparticles to the detection of atherosclerosis . . . 1104
   4.1. Macrophages . . . 1105
   4.2. Endothelial cells . . . 1107
   4.3. Calcifying microvesicles . . . 1107
   4.4. Clinical advances in MNPs for atherosclerosis diagnostic . . . 1108
5. Future perspectives for diagnosis . . . 1108
6. Concluding remarks . . . 1110
   Acknowledgments . . . 1110
   References . . . 1110

1. Introduction

Atherosclerosis is a chronic inflammatory disease, characterized by the formation of a lipid-rich plaque inside the arteries. The formation of atherosclerotic plaques occurs in curvatures and

* Corresponding author.
E-mail address: veronica.lassalle@uns.edu.ar (V.L. Lassalle).

http://dx.doi.org/10.1016/j.biopha.2017.07.012
0753-3322/

branch points of arteries. This situation causes arterial wall thickness, limiting the flow blood to the organs. Despite the advances in the prevention and therapy of cardiovascular pathologies, they are still the first cause of death in the western world.

In general terms; two types of atherosclerotic plaques may be found: one known as stable plaque and other called vulnerable plaque. The former is usually rich in extracellular matrix and smooth muscle cells whereas the vulnerable plaques are rich in macrophages, other inflammatory cells and exhibit a fibrous cap. While stable plaques can be present without causing any damage for years, vulnerable plaques are prone to rupture and release thrombus into circulation causing myocardial infarction and stroke [1,2]. For that reason, an early detection of unstable plaques is primordial in the prevention of these dramatic cardiovascular events.

Several dealings are involved in the initiation and progress of the disease [3]. Initially, the excess of low density lipoprotein (LDL) in the circulation starts to accumulate in the arterial lumen wall, where the lipoproteins suffer modifications such as oxidation, cleavage and aggregation. This process causes a chronic injury to the endothelial cells, activating the inflammatory process through the expression of surface adhesion molecules such as VCAM-1 and ICAM-1, which may recognize monocytes and T lymphocytes. Monocytes differentiate into macrophages and take up the ox-LDL generating foam cells charged with cholesterol. When foam cells died, they release their lipid content and tissue factors causing the formation of a pro-thrombotic necrotic core, which is the key component of unstable plaques [4–6]. Scheme 1 illustrates and summarizes the major events involved in plaque destabilization.

Nowadays, the development of nanotechnology at the health service has opened novel perspectives in relation to the treatment and diagnosis of several diseases [7–9]. The possibility of designing nanoparticles with specific ligands or functional groups, able to preferentially bind and recognize one or more compounds in unstable plaques, appears as an invaluable tool in the early diagnosis of atherosclerosis. The current research trends cover multiple nanosized systems intended as contrast agents for cardiovascular imaging; such as fluorescent, radioactive, paramagnetic, superparamagnetic and multimodal, among others [10].

In this context, the present review is focused on the use of magnetic iron oxide nanoparticles as improved contrast agents for the detection of unstable plaques by Magnetic Resonance Imaging (MRI) as a way to attain the early diagnosis of atherosclerosis.

It is well known that the articles in open literature reporting different aspects and applications of MNPs are abundant [11–13]. In spite of this, the published reports regarding to magnetic nanoparticles for the detection and treatment of atherosclerosis are significantly lower [14–16]. Besides, the present review involves different approach in several points. In first place, the discussion will be restricted to the use of iron oxide magnetic nanoparticles as contrast agents for the mentioned pathology. The aim is to discuss on the most suitable modifications/functionalization for conferring specificity to the magnetic nanoparticles for atherosclerotic plaque detection. Secondly, the importance and the advances in the synthesis of dual modal magnetic nanoparticles will also be addressed.

Hence, this contribution proposes a different view regarding to a very actual topic that has not been addressed from this point of view in the actual literature, at least to the best of these authors knowledge.

2. General aspects of imaging diagnosis, differences between them

In general terms, imaging techniques may be classified in morphological, functional and molecular imaging [17]. While the former shows the final effect of molecular alterations, functional and molecular imaging provide biological information of a disease in a non-invasive way [18–20]. These last techniques have been analyzed in great detail in the context of this Review, because MNPs may be suitable to improve the quality of the image acquired by these techniques.

Molecular imaging is recognized as a powerful technique to detect diseases in the early stages. It is also able to recognize the pathway of a disease monitoring the response to therapy [21,22]. This technique requires two important elements: molecular probes or imaging agents and a hardware to control the probes. Molecular/functional imaging modalities include positron emission tomography (PET) [23], single-photon emission computed tomography (SPECT) [24], computed tomography (CT) [25], fluorescence molecular tomography (FMT) [26], photoacustic tomography (PAT) [27,28] and magnetic resonance imaging (MRI) [29].

Each imaging modality exhibits advantages and disadvantages. A summary of those advantages and disadvantages as a function of each technique is shown in Table 1. For example, PET and SPECT have excellent sensitivity and elevated tissue penetration but low resolution whereas MRI provides high resolution anatomical images and satisfactory tissue contrast. However, it displays low sensitivity and poor tissue penetration. On the other hand, the use of CT may provide high resolution 3D but weak contrast soft-tissue images. This fact justifies the need of designing multi-modal imagining systems as an improved option to obtain molecular images.

The advance of nanotechnology has generated novel kinds of materials highly attractive in the area of molecular imaging. The possibility to design nanomaterials with well-defined and controlled physical and chemical properties represents a great benefit over the traditional contrast agents. Besides, the most

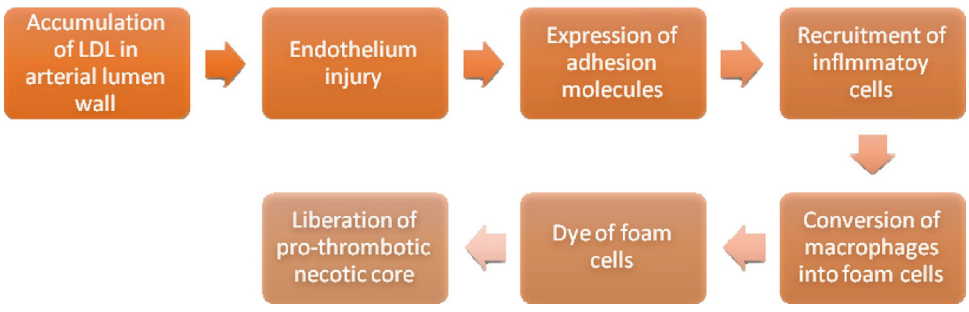

Scheme 1. Principal events involved in the formation of an atherosclerotic unstable plaque.

Table 1
Advantages and disadvantages of Molecular Imaging Modalities.

Imaging Modality	Advantages	Disadvantages	References
MRI	High spatial resolution Good soft tissue contrast	Low sensitivity	[29]
CT	Fast acquisition time Provides 3D images	Weak soft tissue contrast	[25]
PET	High sensitivity Elevated tissue penetration	Exposure to irradiation Low spatial resolution	[23]
FMT	Low cost High sensitivity	Limited spatial resolution	[26]
PAT	High resolution of biological structures, from organelles to organs.	Several diseases manifest insufficient intrinsic PAT contrast.	[27,28]

promissory issue related to the implementation of these nanomaterials is associated to the feasibility to bind specific ligands to their surface, improving their selectivity and, hence shortening the detection times. Among the nanomaterials explored for these purposes, it is possible mention quantum dots, metal nanoparticles, paramagnetic and superparamagnetic nanoparticles, among others [17]. Quantum dots have been used in optical fluorescence and photoluminescence [30]; gold nanoparticles in CT [31] and magnetic nanoparticles almost exclusively in MRI [32].

They have been evaluated for the diagnosis of different pathologies including atherosclerosis.

3. Magnetic iron oxide nanoparticles

Magnetic iron oxide nanoparticles are composed of an inner core of magnetite (Fe_3O_4) or maghemite (γ-Fe_2O_3) and a suitable coating of varied nature depending on the planed applications. When MNPs are exposed to an external magnetic field, their magnetic moments immediately rotate into the direction of this field enhancing the magnetic flux. After the removal of the magnetic field, Brownian motion is sufficient to cause the magnetic moments to randomize; hence their magnetic properties are absent. This behavior is known as superparamagnetism and is only manifested when some magnetic materials are reduced to the nanosizes. Hence, it is a size dependent property.

Because of their high magnetic susceptibility and tailored surface properties, superparamagnetic iron oxide nanoparticles have been extensively investigated for biomedical purposes, for instance, as drug delivery systems [33,34], in bioanalysis [35], hyperthermia [36,37] and as contrast agents for MRI. In order to improve the biocompatibility and avoid particle agglomerations, nanoparticles are commonly coated with polymers, small molecules and surfactants, among others.

Some characteristics such as hydrodynamic diameter, surface charge and the nature and density of the coating are key in determining the viability of nanoparticles in biomedical applications [38]. These parameters strongly affect the possibility of interaction as well as their feasibility to maintain the superparamagnetic behavior [39].

3.1. General aspects of MNPs in diagnosis

MRI technique has evolved as a powerful noninvasive modality for diagnosis. It is based on the application of a magnetic field which produces the alignment of the magnetic moments of protons in the direction of this field. The direction of magnetization changes after the application of a radio frequency. The time until the magnetic moments align to their original position is called relaxation time. Relaxation can be divided into two processes: longitudinal relaxation (known as T_1), transversal relaxation (or T_2). Even when relaxation is tissue dependent and MRI may allow the discrimination of a pathological tissue, the contrast between tissues may not be enough for the diagnosis of diseases. In order to get amplified contrast, exogenous contrast agents, which alter the relaxation times, are used. Although most contrast agents may affect the T_1 and T_2 relaxation, they usually affect preferentially one relaxation time more than the other, so they may be classified as T_1 or T_2 contrast agent [40].

In practice, gadolinium based contrast agents (GBCAs) are the most commonly used ones. They are employed as T_1 contrast agents, providing positive contrast, which is observed as a bright image. Gd is a cytotoxic ion, hence it must be administrated as a chelate combined with large organic molecules. According to their structure, GBCAs may be classified as linear or macrocyclic complexes. The administration of linear Gd complexes in patients with renal deficiency generally leads to a disorder known as nephrogenic systemic fibrosis (NSF) [41]. In such patients the elimination of the contrast agent may take more than 30 h. when in patients with normal renal function the Gd complex is eliminated between 2 h after administration [42]. The persistence of Gd-complexes in the body increased the risk of dechelation. The thermodynamic stability of the chelate would determine the facility of the dechelation process. Clinical approved GBCAs are thermodynamically stable. Macrocylic ligands based on 1,4,7,10 tetraazacyclododecane-1,4,7,10-teraacetic acid (DOTA) exhibit similar thermodynamic stabilities compared to those of the linear diethylenetriamine penta-acetic acid (DTPA) ligands but are more kinetically stable, and are thus a more favourable chelate for Gd (III)-based agents [43].

Recent publications have reported the accumulation of Gd in tissues like brain and bone using both linear and macrocyclic complexes in subjects with normal renal function [44,45]. It is worth noting the these articles do not provide enough information regarding to the nature of Gd accumulated (i.e chelate or to gadolinium ions). However, these observations should be seriously considered when determining the impact of Gd accumulation on the patient's health. Details and more specific information about this topic may be found in a current review [46].

From a comparative point of view, Chen and co-workers have analysed the toxicity of three different T_1 MRI contrast agents in preclinical assays using mouse models. They examined the effect of gadopentatate dimeglumine (a linear complex), manganese oxide and an extremely small iron oxide. Accumulation and lesions in different tissues (liver, spleen, hearth, kidney and lung) were evaluated. The authors concluded that the iron oxide showed a

better safely profile compared with Gd and Mn contrast agents using similar simulated clinical doses for MRI purposes [47].

Even when the risk for NSF is lower using macrocyclic Gd complexes [48], it seems that iron oxide nanoparticles may be a reliable alternative for MRI in patients with different renal failures.

Iron oxide magnetic nanoparticles have been traditionally employed as T_2 contrast agents, giving a negative (dark) contrast image. It was found that superparamagnetic iron oxide nanoparticles may provide a positive contrast in T_1-weighted images, as a function of their sizes [40].

Own recent data further reinforce these findings in demonstrating the efficiency of MNPs as contrast agents of both relaxativity times. We have evaluated the performance of magnetite nanoparticles coated with ascorbic acid (MNPs-AA) as contrast for MRI using a Philips Achieva 1,5T clinical equipment. We have achieved the experiences using a Phantom containing aqueous dispersions of MNPs-AA of known concentrations. Our results in fact coincide with the above described in the sense in that MNPs-AA dispersions resulted efficient to generate contrast in both modalities (T_1 and T_2) employing different measurement sequences. The Fig. 1 shows the MR images generated by MNPs-AA (iron concentration 0,4 mM) using the sequences: TR 700 ms, TE 10 ms, echo 1, NSA 1, thickness 5 mm for bright T_1 contrast; and TR DE 2000 ms, TE 110 ms, echo 1, NSA 1, thickness 5 mm for dark T_2 contrast.

In last years some efforts have been done to produce dual-MRI contrast agents. Some materials composed of Gd-labeled MNPs were reported to be adequate for this purpose. Szpak et al. reported the synthesis of a dual MRI contrast agents consisting of MNPs and gadolinium ions associated to an ionic chitosan layer. The authors studied three synthetic pathways, obtaining two suspensions with adequate characteristics to performed relaxivity measurements. These suspensions showed very good r_1 and r_2 values, which were higher than some commercially available contrast agents [49]. In other work, the synthesis of a core/shell/shell $Fe_3O_4/SiO_2/Gd_2O(CO_3)_2$ was proposed. The diameter of the magnetite core was 12 nm and the thickness of the $Gd_2O(CO_3)_2$ was about 1,5 nm. Different thickness of silica shell (8–20 nm) was studied to determine their impact in the magnetic properties of both contrast agents. The higher the size of the silica shell, the better performance in the T_1 effect was achieved. The major distance from the T_2 contrast agents reduce the perturbation of it over the T_1 effect. The evaluation of the dual-MRI contrast agent was achieved under T_1 and T_2-weighted images and through the calculation of r_1 and r_2 relaxation time [50]. Another study has investigated the potential of the dual T_1- and T_2 mode MRI acquisition using MNPs through longitudinal comparison and optimization of two contrast sequences such as Fast Low-Angle Shot (FLASH) and ultrashort echo-time (UTE). The authors informed that the precise control on the magnetic particle size (whose magnetic core was estimated in aprox. 7 nm) was the key factor for the efficiency as dual-contrast agent [51]. In such study the authors informed that SPION they used were not yet clinically approved. On the other hand, chemically equivalent iron oxide nanoparticle (Feraheme, AMAG Pharmaceuticals, Lexington, MA, USA) has been clinically approved for the treatment of iron-deficiency anemia and also applied in MRI. Further similar characterization of dose dependent MR contrast properties of these nanoparticles may facilitate the clinical applications of dual-contrast acquisition method described in this study [52].

3.1.1. MNPs in the market

Several commercial products based on MNPs have been in the market, mainly as contrast agent for MRI. The most important are listed in Table 2.

However, nowadays only a cup of them remain available in the market. The reasons exposed in the published articles are varied. For instance, in the case of Feridex, its developer (AMAG

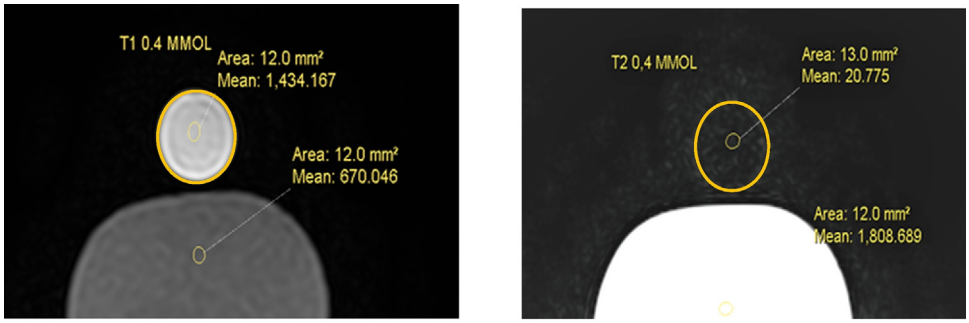

(a)

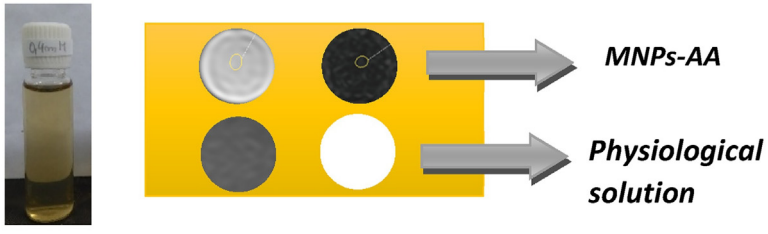

(b)

Fig. 1. (a) Laeft, T_1-weighted images of MNPs-AA (iron concentration 0,4 mM) compared with physiological solution. Right, T_2-weithed images MNPs-AA compared with physiological solution. (b) Images of Ascorbic acid coated magnetic nanoparticles (MNPs-AA; iron concentration 0,4 mM) and physiological solution (PS). Left, T_1-weighted images of MNPs-AA and PS. Right, T_2-weithed images of MNPs-AA and PS.

Table 2
MNPs approved to their commercialization in the health field.

Commercial name	Country and year of approbation	Size (nm)	Biomedical interest-others	Refs.
Ferumoxytol (Feraheme),	(2009-6-30)FDA	30	Treatment of iron deficiency anemia Ferumoxytol contrasted MRI is used in primary tumor, cancer lymph node metastasis.	[53]
Ferumoxides (Feridex)	August[a] 30th, 1996 by FDA	120–180	Initially as MRI contrast medium for the detection of liver lesions.	[54]
Ferucarbotran (Resovist)	Approved for the European[b]market in 2001	60	Organ-specific MRI contrast agent, for the detection of especially small focal liver lesions.	[55]
Ferristene (Abdoscan) and ferumoxsil (Lumirem or Gastromark)[c]	Gastromark approved by FDA in 1996	300	Used for gastrointestinal as a magnetic ironparticle solution.	[56]
Ferumoxtran-10 (Combidex or Sinerem)	Approved in USA and Europe	20–50	Used to detect metastatic disease in lymph nodes.	[57]

[a] Discontinued.
[b] Production of Resovist has been discontinued in 2009.
[c] Actually unavailable.

Pharmaceuticals,Inc.) decided to discontinue it. Although it is less competitive in intravenous contrast agent markets, their application in active cell tracking by MRI is recognized. On the other hand, the production of Resosvist, has been discontinued in 2009 due the successful market introduction of Primovist (Gd-DTPA), another liver imaging agent of Bayer Schering Pharma AG. Ferristene and Ferumoxsil were gradually eliminated by the market because of negative profit though they demonstrated to be effective and safe.

In spite of this apparently negative panorama regarding to the commercial availability of MNPs, it was found that the registration process of Combidex in Europe was withdrawn by the manufactured, but, in 2013 the Radboud University Medical Center obtained the rights and documents of Combidex. In 2015 the rights were transferred to SPL medical B.V. in The Netherlands and Combidex is manufacturing again. It is currently using in that country to detect small metastatic lymph nodes in patients with prostate cancer [57].

Furthermore, several similar nanosystems are actually FDA approved clinical trials (visit www.clinicaltrials.gov). For instance, there are four approved clinical trials using Endorem to track monocyte or inflammation cell (mainly indicated one kind of monocyte—macrophage) and a phase 2 study using Feridex to track adult bone marrow derived stromal cells (MSC) for severe cases of Multiple Sclerosis therapy. Besides, another ferucarbotran (Supravist) with smaller size than Resosvist is nowadays under clinical phase 3 study by Bayer Schering, as a positive enhancing blood pool agent. Furthermore, a derivative of Ferumoxtran is being tested in a new application involving imaging of brain tumors especially with reactive inflammatory cells, taking advantage of its long plasma half-life and imaging ability of blood–brain barrier's abnormal site. (www.clinicaltrials.gov).

In this scenario it is clear that Gd based formulations are still dominating the contrast agent market. However, judging by the available literature and recent clinical trials proofs, the future of MNPs is highly promissory for both diagnosis and imaging guided therapy with the suitable incorporation of specific ligands to well defined pathologies [58–60].

3.2. Principal techniques to prepare MNPs for biomedical applications

Available methods to synthesize iron oxide-based nanoparticles are abundant in view of the published scientific articles [61,62]. Here, only the most relevant and suitable from the biomedical applications are recompiled, since a detailed description of them is out of the scope of this article. For more in deep information in this regard recent contributions devoted to the synthesis and properties of MNPs may be revised [63–65].

The co-precipitation method is one of the most widely used because of its simplicity, easy handling procedure, low cost and low time consuming. It involves the addition of a base (usually NaOH or NH_4OH) to an aqueous solution of Fe^{3+} and Fe^{2+} in a molar ratio 2:1. The precipitation of magnetite occurs at pH between 9 and 14 as long as the molar ratio between the iron salts is maintained. To ensure this condition, the procedure is commonly carried out under inert atmosphere. Magnetite formation is evidenced by the appearance of a black solid. In order to avoid particles aggregation, the reaction is normally heated in presence of adequate surfactants/and/or stabilizers such as oleic acid, sodium dodecyl sulphate, among others. The overall reaction is the following:

$$Fe^{2+} + 2Fe^{3+} + 8OH^- \rightarrow Fe_3O_4 + 4H_2O$$

In spite of its simplicity, this methodology presents limitations associated to the lack of control regarding to size dispersions. Our own researches as well as other groups's work demonstrated that it is possible to reach greater control over the interest properties, including size, by conveniently adjusting experimental parameters. The stirring velocity, the kind of base, the addition order of the chemicals reactants, the type of atmosphere (inert or air) and the temperature have an impact on the size, shape and dispersion ability of the MNPs [66–70].

Hydrothermal method is another well-known technique to prepare iron oxide-based nanoparticles. This synthesis is performed in aqueous media in autoclave or reactors at high temperature and pressure. These conditions enable a rapid nucleation step and the growth of the formed nanoparticles is also faster. This mechanism favors the formation of MNPs with low sizes. Although the main factor regulating the size appears to be the reaction times; other factors, such as temperature, nature of solvent, the addition of seeding and the precursors seem to have an impact on size [71–73].

Nanoparticles with suitable characteristics such as narrow size distribution, highly crystalline and monodisperse could be obtained by thermal decomposition of the iron precursor in a hot reaction mixture [74]. Thermal decomposition takes place in two phases: the formation of the nuclei, at around 200 °C and its grown at the boiling temperature of the solvent [75]. Size and shape may be controlled adjusting parameters like iron precursor, the stabilizer and its concentration and the used solvent [76–78]. The nanoparticles obtained by this method are usually hydrophobic, being necessary an additional step to re-dissolve them in aqueous solutions.

The sol-gel method is also commonly used to synthesize MNPs. It is based on the hydroxylation and condensation of precursors in

solution originating a "sol" of nanometric particles. After the removal of the solvent a three dimensional metal oxide network is obtained. Polyols such as ethylene glycol or propylene glycol are usually used to control particle growth, preventing the aggregation [79,80]. These materials are either toxic or expensive, so that modified sol-gel methods avoiding the use of them, have been recently investigated [81].

Fundaments of sonochemical methods lie on the chemical effects produced by acoustic cavitation. Acoustic waves create oscillating bubbles which accumulate ultrasonic energy. Once the bubbles reach a certain size, they collapse realizing the accumulated energy. As a result, high temperature (about 5000 K), pressure (1000 bar) and a high cooling rate are generated; creating extreme reaction conditions and making the sonolysis an attractive alternative to synthesize magnetic nanoparticles [82]. Enomoto and co-workers prepared magnetite nanoparticles in a solution of ethanol-water from $Fe(OH)_2$ precipitate under ultrasonic irradiation [83]. They found that this methodology renders monodisperse MNPs that may be obtained in shorter times compared with mechanical stirring. The MNPs obtained by ultrasound showed better magnetic properties than the nanoparticles obtained by mechanical stirring. The alcoholic solvent as well as the proportion water/alcohol are the factors determining the achieved particle size [84].

A recently reported method to prepare MNPs is microwave-assisted synthesis. This technique involves low reaction times, allowing satisfactory control over the MNPs size. Early reports on this regard were mainly focused on the achievement of the nanoparticles rather than in the study of its properties such as the colloidal stability [85–88]. Nonetheless, currently research is considering the preparation of MNPs by microwave synthesis for biomedical applications. The coating of the nanoparticles with biocompatible materials as well as size distribution were well evaluated in such articles [89–91].

Other less explored methods to obtain MNPs may be found in open literature, i.e: aerosol/vapor – phase methods, electrochemical methods, microemulsion and biosynthesis [62]. Table 3 summarizes the advantages and disadvantages of the main techniques used to prepare MNPs.

3.3. Different coating and strategies to assess stable MNPs in dispersion

MNPs have to meet a number of requirements in order to be suitable for biomedical applications, including diagnosis. Among them, the most important are size distribution (that must be almost monodisperse), superparamagnetism and a specific surface functionality provided by a coating (Scheme 2).

In terms of the size, it determines the transport of nanoparticles into the tissues. If nanoparticles are too large, they will be taken by liver and spleen, shortening blood circulation time. If the nanoparticles are too small (less than 8 nm) they will be more likely filtrated out through the kidneys. Therefore, for clinical proposes nanoparticles between 10 and 300 nm are commonly accepted as efficient [100].

MNPs may be classified in super-paramagnetic iron oxide nanoparticles (SPIONs), when the diameter ranged from 50 to 100 nm, and ultra-small super-paramagnetic iron oxide nanoparticles (USPIONs), when the average size is less than 50 nm, including coating. After intravenous injection, SPIONs are removed from the blood by the mononuclear phagocytic system (MPS). The uptake of the nanoparticles is mainly observed in liver, spleen, bone marrow and lymph nodes. Because of this, MNPs have been firstly studied as contrast agents to imagining liver and spleen [101]. On the other hand, USPIONs, generally avoid the massive uptake by macrophages of the MPS, due to their very small size, enhancing their circulation time [102]. Hence, USPIONs can reach macrophages in deeper compartments.

Three kinds of interactions may be distinguished among magnetic nanoparticles: London-Van der Waals interactions, magnetic forces and interactions of the electrical double layer. In order to obtain stable nanoparticles, the first two attractive forces must be counteracted by the repulsive forces. Since these last are less intense, nanoparticles are treated to modify their surface in order to increase their stability in dispersion in the media of interest (aqueous or organic) by strengthen the repulsive forces. The modification/functionalization of MNPs is a widespread topic that besides, has been extensively reviewed in recent

Table 3
Comparison between most common methods to prepare MNPs.

Method	Advantage	Disadvantage	Refs.
Co-precipitation	Simplicity Low cost	Lack of size control	[66,92]
Hydrothemal	Control of the geometry and size after optimization of the experimental parameters	Slow reaction kinetic	[71,73]
Thermal decomposition	Size and morphology control. Uniform size distribution	Hydrophobic NPs are obtained	[74,75]
Sol-gel	Good control of particle size and shape	Expensive and sometimes toxic reagents are needed.	[79]
Sonolysis	Acceleration of reaction rates Reduction of crystal growth	Lack of control of the shape and dispersability	[84,93]
Microwave	Control of size and shape Fast and energy efficient	Equipment availability	[94]
Aerosol/vapor	Small nanoparticles with narrow size distribution are achieved	Expensive equipment Low product yield	[95]
Electroquemical methods	Control on nanoparticle size	Low purity MNPs	[96]
Microemulsion	MNPs with uniform size distribution are achieved	Difficult to scale-up	[97]
Biosynthesis	Green method High product yield Good reproducibility	Slow rate of synthesis	[98,99]

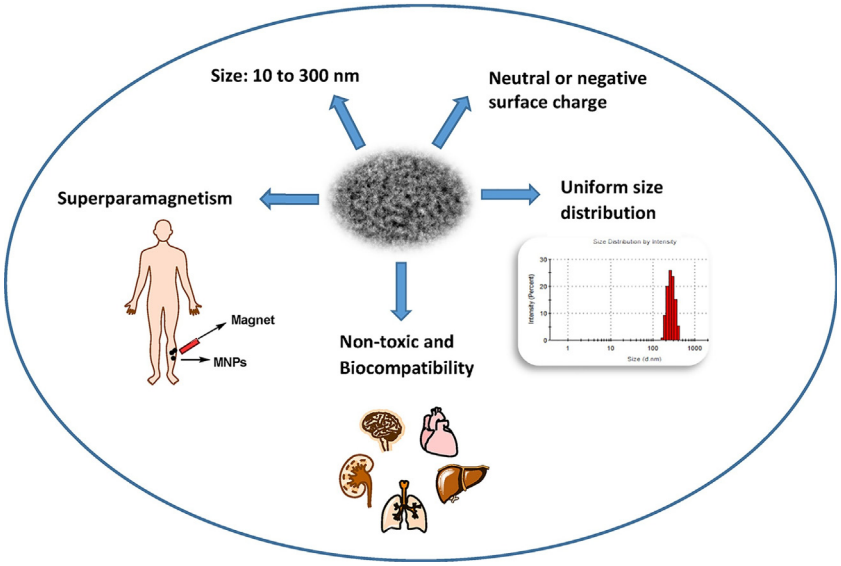

Scheme 2. Requirements for MNPs intended for biomedical applications.

literature [39,103,104]. Hence only a brief description is here provided according to the main focus of this Review.

The coating may be achieved by incorporating the additives (stabilizer and/or functionalizer) during (in situ) or after (post-coating) the synthesis of magnetic nanoparticles. Another different strategy is promoting the additive exchange. The latest method is based on the high affinity of hydrophilic additives for the iron oxide surface. In a mixture with a high concentration of a hydrophilic functionalizer and/or stabilizer, a hydrophobic additive would be displaced from the MNPs surface.

Most common coatings used to stabilize MNPs may be classified in three groups: polymers, monomers and inorganic compounds. In general, polymeric moieties induce nanoparticles stabilization through steric repulsion. On the other hand, organic monomers present functional groups like carboxylates, sulfates and phosphates providing electrostatic surface stabilization. Both stabilization mechanisms are illustrated in Fig. 2(a).

Fig. 2(b) depicts a photograph of synthesis of MNPs coated with ascorbic acid (MNPs-AA), as example of a monomeric stabilizer. In this case the AA was added in situ during the co-precipitation procedure in our labs. Besides, a TEM micrography of an aqueous dispersion of MNPs-AA is included.

The stabilization with inorganic materials such as gold or silica results in a core-shell like structure with magnetic nuclei as it is represented in Fig. 2(c). The surface modification of nanoparticles has a dual purpose: by one side, to achieve colloidal stabilization; and on the other hand, to improve biocompatibility and blood circulation half time. For example, the functionalization with PEG reduces the non-specific uptake by macrophages enhancing the time of nanoparticles in blood stream [105]. In addition, surface modification may allow the conjugation of MNPs with proteins or antibodies, which is very important to achieve an active targeting. Table 4 shows the substrates commonly employed as coating of MNPs intended for biomedical applications.

4. Magnetic nanoparticles to the detection of atherosclerosis

Nowadays, it is known that the composition of the plaque is the main factor determining its stability, even more than the stenosis degree [123]. Morphological imaging techniques such as Magnetic

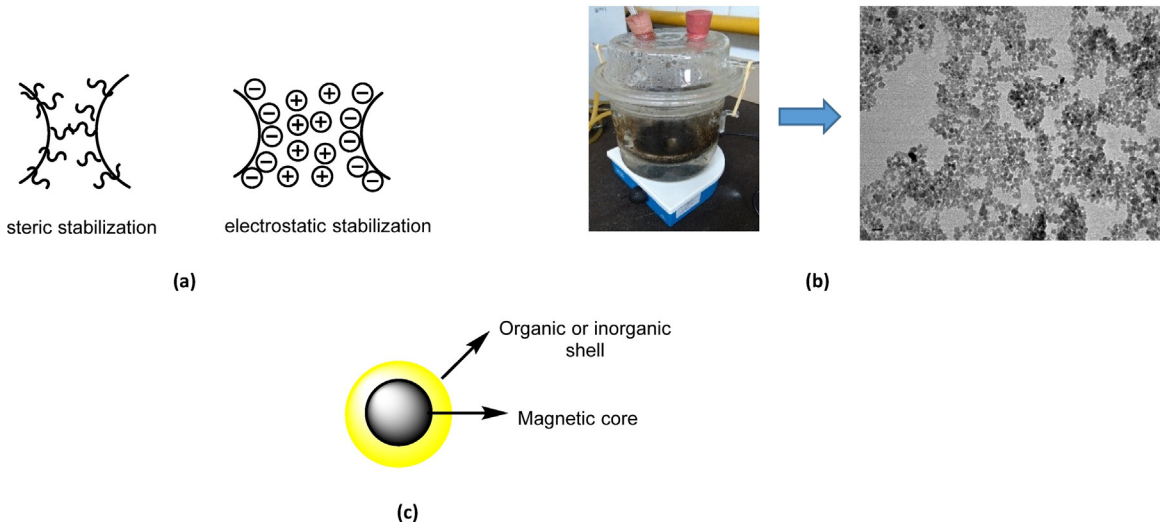

Fig. 2. (a) Representation of different stabilization mechanisms conferred to the coatings. (b) Images of synthesis of AA-MNPs by co-precipitation,a stable aqueous dispersion of AA-MNPs and TEM image of the same formulation. (c) Scheme of MNPs coated silica.

Table 4
Atherosclerotic targets as a function of the ligands to conjugate on MNPs.

Type of coating	Specific coating	Application	Refs.
Polymers	Dextran	MRI contras agent	[106]
	Carboxymethyl dextran	MRI contrast agent	[107]
	Chitosan	Hyperthermia	[108,109]
		Drug delivery	[110–112]
	Polyethylene glycol	Pharmacokinetic studies	[113]
Monomers	Citric acid	MRI contrast agents	[114,115]
		Hyperthermia	[116,117]
	Ascorbic acid	MRI contrast agents	[118,119]
	Oleic acid	Hyperthermia and MRI contrast agents	[120]
Inorganic materials	Gold	Several biomedical applications	[121]
	Silica	General biomedical applications	[122]

Resonance Angiography (MRA) and Computed Tomography Angiogram (CTA) give information about intraluminal stenosis generated by plaque growing, but fail in detecting the presence of unstable plaques. On the other hand, molecular imaging, in a non-invasive way, allows a biological understanding of atherosclerotic plaque [20,124]. Thus, this technique would be able to supply early detection of a vulnerable plaque, and thus would provide a better care of patients suffering this pathology.

Nanosystems for molecular imaging of atherosclerotic plaques have been developed taking into account the different molecular markers involved in the progression of the pathology. Fig. 3 illustrates the main components of a vulnerable atherosclerotic plaque. Among the molecular markers, endothelial molecules such as VCM-1, ICAM, E- and P-selectins are attractive targets. Macrophages are also considered suitable targets since they constitute a major component of such plaques. As the deposition of fibrin is one of the earliest signs of plaque disruption, the detection of this component is very important. In an advanced plaque, a process of angiogenesis takes place due to the growing metabolic needs. This process of neovascularization is associated with the expression of integrin $\alpha_v\beta_3$, which is another interesting target [14].

As it has been previously described, several molecular imaging techniques may be found for clinical applications. Nanosystems devoted to MRI as contrast agents have been the most widely explored regarding to atherosclerosis detection. However, the development of nanoparticles for other imaging modalities has been increased. Gold nanoparticles have been designed for enhanced CT imaging in macrophages accumulated in unstable atherosclerotic plaques [125,126]. Atherosclerosis has been evaluated through PET using different tracers like ^{18}F-fluoro-D-glucose, radiolabeled choline, among others [127]. Radiolabeled nanoparticles intended for atherosclerosis diagnosis have been developed as multimodal imaging. That means they provide imagining not only by PET but also by CT [128,129] or MRI facilities. There are some challenges in the design of radiolabeled nanoparticles for biomedical applications since the nanoparticle structure and the radiolabeling must be stable in the physiological medium. Moreover, the half-life of the radionucleotide needs to be long enough to reach the target [130]. The design of nanoparticles for imaging atherosclerosis through more than one imaging modality is a growing area of study because of multiple reasons. Among them, the most important ones rely in the possibility to overcome the disadvantages of each technique; as well as in increase the functionality of the contrast agents.

The next sections will consider the studies involving the synthesis and modifications of MNPs to specifically target one component of unstable atherosclerotic plaques.

4.1. Macrophages

Macrophages are one of the most utilized targets in molecular imaging. These cells are able of internalizing foreign bodies and play an important role not only in the development of the atherosclerotic plaque but also in many other diseases like obesity, rheumatoid arthritis and diabetes [131].

Macrophages are the major contributors to the inflammatory response through the secretion of pro-inflammatory mediators. Hence, a high concentration of them in atherosclerotic plaques is an indicative of plaque destabilization. According to the type of activation (classical or alternative), macrophages may be distinguished in M1 macrophage, which produce pro-inflammatory cytokines and reactive oxygen and nitrogen species; and M2 macrophage, which contribute to tissue repair and secrete anti-inflammatory factors.

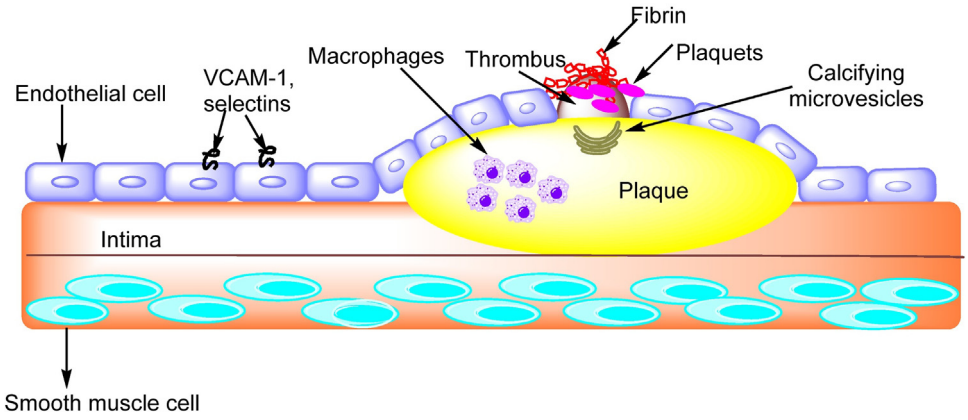

Fig. 3. Representation of a vulnerable atherosclerotic plaque including the possible targets for its detection.

Macrophages may uptake nanoparticles and other foreign bodies through different process: pinocytosis, receptor-mediated endocytosis (for example scavenger receptors) and phagocytosis. The latter is a common process to engulf large particles. Raynal et al. have concluded that the uptake of Ferumoxides (MNPs-coated with dextran) occurs through a scavenger receptor SR-A [132]. This is one of the six subgroup of scavengers receptors (the group included also the CD36, lectin-like oxidized LDL, SR-B1, CD68 and MARCO receptors). The subtype SR-A and CD36 are both involved in the process of atherogenesis and atheroinflammation [133]. Although, the accumulation of MNPs in macrophages has been observed, the mechanism of uptake remains not clear enough [134]. The uptake procedure is variable regarding the size and nature of the coating.

Plaque macrophages highly express the scavenger receptor type A (SR-A). This receptor (which is not found in normal vessel walls) mediated the uptake of oxidized lipoproteins and is greatly expressed in a lipid rich environment. SR-A receptor, has specificity for polyanionic macromolecules such as maleylated bovine serum albumin (mal-BSA), malondialdehyde modified LDL and poly-inosinic acid. The coating of MNP with dextran sulfate (SDIO) has been reported as a suitable strategy to favor the target of this receptor. Dextran coated USPIONs and SPIONs are known to undergo spontaneous uptake by macrophages through phagocytosis. This mechanism of accumulation is quite inefficient and requires high doses and time from injection to achieve a suitable contrast between the plaque and the surrounding tissues. However, coating the magnetic nanoparticles with dextran sulfate instead dextran, leads to nanoparticles that may be recognized by the SR-A receptor [135]. SDIO was achieved by treated dextran-coated nanoparticles with SO_3-pyridine complex under argon atmosphere, in presence of 2-methyl-2-butene which acts as an acid scavenger. The obtained monodispersed nanoparticles presented an average hydrodynamic size of 62,4 nm. In order to confirm that the uptake of dextran sulfate coated magnetic nanoparticles occurs though the SR-A receptor, a competitive study in P388D1 murine macrophage cells was performed. This experiment showed that increasing the concentration of dextran sulfate (ligand of SR-A), the uptake of SDIO decreases, whereas in presence of increasing concentrations of dextran (no ligand of SR-A) the uptake of SDIO remained unchanged. These situations proved that macrophages take up SDIO through the scavenger receptor. The study on Apo $E^{-/-}$ mice revealed a considerable decrease in MRI signal of the ligand carotid 4 h after the injection of the nanoparticles for SDIO. At this time, SDIO provided an increment of 4-fold in the contrast ratio, in comparison with DIO. The last one needed 24 h after the injection to produce a sizeable signal lost. The *in vivo* study confirmed the preferential accumulation of SDIO in atherosclerotic plaque because they are taken up by macrophages through a receptor-mediated process [135].

You and co-workers also prepared dextran sulfate-coated iron oxide nanoparticles, with modifications in order to ensure a complete decoration of MNPs with dextran sulfate. They designed a copolymer with a dextran sulfate segment for its recognition by the SR-A receptor on the activated macrophage (DS-*b*-poly (glycerol methacrylate)) and a PGMA (poly(glycidyl methacrylate) to anchor in the MNP unit. This allowed the synthesis of SDIO in one step using the co-precipitation method. The obtained nanoparticles exhibited a hydrodynamic size of 64 nm; whereas cellular uptake evaluation in vitro was assessed using RAW264.7 murine macrophages cells. In this study, the ability to take up the nanoparticles of activated and inactivated murine macrophages was compared with bovine aortic endothelial cells (BAEC) which do not express SR-A receptor. Prussian blue staining assay showed that MNPs were present in activated and inactivated murine macrophages but blue spots were higher in the activated ones. The greater uptake of SDIO in activated macrophages was confirmed in *in vitro* MRI images, since the highest contrast effect was observed using these conditions [136].

Activated macrophages in atherosclerotic plaques also highly express hyaluronic acid (HA) receptors stabilin-2 and CD44 [137]. In this concern, HA has been recently reported as a coating of magnetic nanoparticles. The nanoparticles were prepared by precipitating iron precursors in the presence of dextran and, in a second step, coated with HA [138]. They exhibited hydrodynamic size of about 205 nm and retained the native biological recognition of HA by CD44; allowing the uptake of macrophages. This was confirmed by means of *in vitro* studies. The same authors reported later the synthesis of HA coated MNPs with smaller hydrodynamic size (about 45 nm). They achieved these results by controlling the amount of dextran used as coating. The dextran-coated-iron oxide nanoparticles were functionalized with amines. Then the HA was attached through amide bond. Thirty minutes after the administration of the HA-coated nanoparticles, (dose: 0,21 mg Fe/kg body) to New Zealand white rabbit, a decrease of the signal in the aorta wall in T_2^* weighted-images was observed. The signal in the lumen also decreased but in less magnitude than in the aorta wall, suggesting that nanoparticles were concentrated in vessel walls [139].

Tsuchiya et al. have prepared USPION and SPION coated with mannan (M-USPION or M-SPION) in view that the mannose receptors of M2 macrophages are more intensely expressed in atherosclerotic plaques than in the adjacent zone. This polysaccharide consists of units of mannose which are recognized by the receptor. The nanoparticles were prepared using the co-precipitation method, adding the mixture of iron salts to an aqueous solution of mannan. Internalization of M-SPION and M-USPION was tested using a rabbit model demonstrating that these MNPs were more internalized by macrophages than dextran coated nanoparticles. Interestingly, there was almost no difference in the uptake of M-USPION and M-SPION. Although the doses used in this work were too high for clinical applications, this study may be considered as a starting point to future investigations regarding to the use of mannose receptor in macrophages for imagining atherosclerosis [140].

Folate receptor β (FR-β) is another interesting target for the detection of vulnerable plaques because it is expressed on activated macrophages but it is not expressed in non-activated macrophages or other immune cells. Jager and co-workers

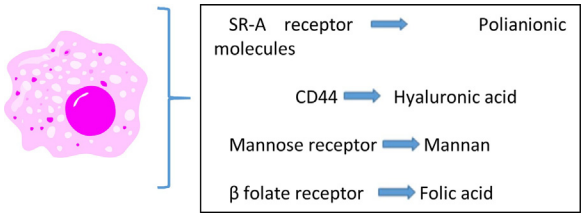

Scheme 3. Schematic representation of the receptors overexpressed on activated macrophages and the possible ligands for atherosclerosis diagnosis.

incubated human carotids samples with folate-FICT (fluorescein isothiocyanate). Ex vivo fluorescent imaging showed that folate-FICT accumulated in areas of high number of activated macrophages [141]. The overexpression of this receptor in activated macrophages has recently led to the development of iron oxide nanoparticles conjugated with folic acid for the diagnosis of rheumatoid arthritis [142]. Although intended for arthritis diagnosis, these nanoparticles could be used for other inflammatory diseases like atherosclerosis. Scheme 3 represents the receptor overexpressed in activated macrophages and their possible ligands for atherosclerosis diagnosis.

4.2. Endothelial cells

Cellular adhesion molecules are key mediators in the development of atherosclerosis since they are involved in the recruitment of inflammatory cells from circulation [143]. The adhesion molecules involved in the atherosclerotic process are: selectins (P, E and L), intercellular adhesion molecules (ICAM), vascular cell adhesion molecules (VCAM-1) and integrins.

The VCAM-1 molecule is expressed on endothelial cells, macrophages and smooth muscle cells in atherosclerotic plaques. They represent an interesting target to identify early stages of the pathological process because they are involved in the inflammatory initiation and progression of atherosclerosis. Kelly et al. modified magnetofluorescent nanoparticles with the peptide VHSPNKK, which has a high binding ability to VCAM-1. Intravenous administration of the fluorescent labeled peptide results in its quick leakage. On the other hand, MNPS modified with the peptide showed better pharmacokinetics, without affecting the specificity for VCAM-1. MNPs which were not modified with VHSPNKK did not show affinity for VCAM-1 molecule. This was the first report regarding to endothelial molecules targeted without the use of antibodies [144].

In a more recent work, USPION have been coated with PEG and a VCAM-1–binding peptide. Conjugation of MNPs with the VCAM-1 cyclic peptide was achieved through a *gem*-bisphophonate compound. These nanoparticles (with a hydrodynamic size of 26 nm) accumulated in early and advanced atherosclerotic plaques on ApoE$^{-/-}$ mice (determined by Prussian blue staining). However, nanoparticles accumulation was not observed in control mice. When PEG- USPION without the binding peptide was used in the ApoE$^{-/-}$ mice studies, iron depositions were not detected. MRI measurements were performed 24 h after the administration of the USPION-VCAM-1 and USPION-PEG. The ApoE$^{-/-}$ mice treated with the former showed a significant signal intensity in the aortic root, while no significant results were observed in mice treated with USPION-PEG [145]. These studies position the VCAM-1 molecule as a possible target for the detection of a vulnerable atherosclerotic plaque.

Another interesting target is P-selectin, an adhesion molecule which is overexpressed on the surface of activated platelets and endothelium. Magnetofluorescent nanoparticles covalent coupled to VH10 antibody (VH10-VUSPIO) were developed to target P-selectin [146]. The overall synthetic pathway involved the modification of maghemite core with PEG and dextran (hydrodynamic radios: 80 nm). The next steps comprised the label with rhodamine and the conjugation with the antibody. Data arising from microscopic images and T_2 and T_1 relaxation rates revealed that these nanoparticles showed specificity for activated platelets while accumulation was not almost observed in the normal ones. The authors demonstrated that 1000 VH10-USPION per platelet was enough to induce a reduction value of T_2 of 50%. Studies on ApoE$^{-/-}$ mice also revealed a reduction on T_2-weighted Images 24 h post-injection due to the accumulation of the targeted magnetic nanoparticles on the activated platelets. In another study by Jacobin-Valat, magnetic nanoparticles were coupled with a recombinant human antibody rIgG4 TEG4 [147]. In this case, maghemite core was functionalized by an aminated polysiloxane film imbibed in a dextran corona and then conjugated with the antibody using SM(PEG)$_{24}$ as coupling agent. These nanoparticles also accumulated selectively around activated platelets [147].

Other strategies to develop contrast agents images for P-selectin consist in covering magnetic nanoparticles with mimics of sialyl Lewis X (SLe^x), the natural ligand of P-selectin. Several mimics are also natural compounds such as fucoidan, a sulfated polysaccharide. To obtain a suitable contrast agent, maghemite was covered with carboxymethyldextran and then coupled with aminated fucoidan. The resulted USPION exhibited a hydrodynamic diameter of about 50 nm and acted as a competitor of the anti-P-selectin antibody. Moreover, magnetophoresis experiment confirmed that fucoidan covered USPION were attached to platelets. Although *in vivo* experiments were not included in this contribution, the obtained results situate fucoidan-USPION as a promising tool for imagining vulnerable plaques [148].

Fucoidan-USPIONs have been evaluated to visualize intravascular thrombi in rat aneurysm, requiring only 30 min visualizing them by MRI. Based on these results, the use of natural ligands, like fucoidan, seems to be a more convenient way to imaging P-selectin than the use of antibodys, which greatly elevate the cost of the nanoparticles synthesis [149].

4.3. Calcifying microvesicles

Calcifying microvesicles are indicators of plaque instability. Wagner et al. demonstrated that the accumulation of citrated coated superparamagnetic iron oxide in atherosclerotic plaques correlates with the presence of calcifying microvesicles. The nanoparticles produced a signal lost intensity in atherosclerotic lesion on vessel wall of WHHL rabbits only 1 h after intravenous

Table 5
Atherosclerotic targets and the ligands conjugated to MNPs.

Ligand	Target	Incorporation of the Ligand	Hydrodinamic radius (nm)	*In vivo test*	Refs.
Dextran sulfate	Macrophage receptor SR-A	Modification of SDIO with SO_3	62,4	On ApoE$^{-/-}$ mice	[135]
Dextran sulfate	Macrophage receptor SR-A	Through a polymer synthesis	64	–	[136]
Hyaluronic acid	Macrophage receptor CD44	Through amide bond	45	On rabbits	[139]
Mannan	Macrophage mannose receptor	Mixing mannan with iron salts	55	On rabbits	[140]
Peptide VHSPNKK	VCAM-1	Derivatization with disuccinimidyl suberate	32	On ApoE$^{-/-}$ mice	[144]
VCAM-1 peptide	VCAM-1	Conjugation through amino-PEG	26	On ApoE$^{-/-}$ mice	[145]
VH10-antibody	P-selectin	Using Sulfo-SMCC as coupling agent	80	On ApoE$^{-/-}$ mice	[146]
rIgG4 TEG4-antibody	P-selectin	Using SM(PEG)$_{24}$ as coupling agent	7,5*	On ApoE$^{-/-}$ mice	[147]
Fucoidan	P-selectin	Through amide bond	50	–	[148]
Citric acid	Calcifying microvessels	–	7	On rabbits	[150]

*The size corresponded to the magnetic core.

administration. The authors proposed that MNPs coated citric acid target the microvesicles due to the chelating capacity of glycosaminoglycns (GAGs), which are negatively charged carbohydrates based on amino sugar dimers and are linked to atherosclerotic calcifications. In vivo, the citrate coating could be replaced because of the interaction of iron oxide with GAGs [150].

In order to explore the capability of other acids to the same purpose, dimercaptosuccinic, etidrionic, tartaric and malic acid were employed as coating of magnetic nanoparticles. The data reveal that MNPs-dimercaptosuccinic acid did not accumulate in atherosclerotic plaques but mainly in heart muscle. As a difference, magnetic nanoparticles coated with the other three acids accumulated in aortic walls in an apoE$^{-/-}$ mice model. The authors explained that the nanoparticles used could enter in the plaque via diffusion through the dysfunctional endothelium. However, the accumulation of these last nanoparticles was lower than the accumulation of citrated-iron oxide nanoparticles. The presence of tartaric, malic and ethidrionic acid-coated magnetic nanoparticles was detected in macrophages and endothelial cells by TEM. In spite of the major *T2*-relaxivity obtained with malic acid, the contrast effect achieved in the plaque was not improved with respect to the NPs coated with other acids. Therefore, the use of alternative acids did not enhance the performance achieved when citrate was employed as coating. In this study citric acid coated-MNPs showed high accumulation in atherosclerotic plaques of Apo E$^{-/-}$ mice 3 h after the intravenous injection [151].

Table 5 summarizes the different targets that have been considered to synthesize MNPs for atherosclerotic vulnerable plaque detection.

4.4. Clinical advances in MNPs for atherosclerosis diagnostic

Existent clinical trials involve the use of MNPs as contrast agents to detect and characterize atherosclerotic plaques; relying on the base of the specific incorporation of magnetic particles by activated macrophages [152]. A study by Kooi et al. [153] performed on 11 symptomatic patients scheduled for carotid endarterectomy, demonstrated that MNPs accumulated predominantly in macrophages in ruptured and rupture-prone atherosclerotic lesions, whereas hardly any particle was taken up in stable plaques [153].

Other clinical assays developed by J.H. Gillard and col. confirmed the capability of MNPs – enhanced MRI to recognize plaque inflammation by accumulation of nanoparticles within macrophages in stenotic carotid plaques [154]. In that study, areas of signal intensity reduction, corresponding to MNPs- and macrophage-positive histological sections, were observed in 7 of 8 patients administrated with similar doses of ferumoxtran. These data were later validated on 30 symptomatic patients scheduled for carotid endarterectomy, showing MNPs enhancement in 90% patients with severe stenosis [155].

More recently, ferumoxytol (Feraheme) based on MNPs of around 20–40 nm coated with poly- glucose sorbital carboxymethylether emerged as other viable option. In the recent NIMINI-2 clinical trial ferumoxytol injection combined with mutiparameter-MRI successfully delimited infarction area, as well as the *peri*-infarct zone in patients suffering from acute myocardial infarction [156]. This should be confirmed with the results of another clinical trial [157].

The main limitation associated to these nanosystems is related to the accumulation times. In such cases the times ranged 24–72hs. after injection. Therefore, the incorporation of suitable ligands to induce an active targeting is still a challenge between medical/scientific communities devoted to this field research (source: http://www.mr-tip.com/ and http://www.clinicaltrials.gov/).

5. Future perspectives for diagnosis

Despite MRI offers satisfactory images of soft tissues with high spatial resolutions, its sensitivity is quite low. The lack of sensitivity represents a problem since atherosclerotic disease may occur anywhere in the vascular system. In this context, the development of nanoparticles combining MRI and others more sensitive techniques, such as PET, is becoming a more suitable and efficient alternative for atherosclerosis diagnosis.

Jarrett et al., developed a multimodal nanoparticle (for MRI and PET) to non-invasively map the distribution of macrophages *in vivo* [158]. Dextran coated iron oxide nanoparticles were cross-linked with epichlorohydrin and then aminated to generate a stronger nucleophile. Afterwards, the nanoparticles were conjugated with the ^{64}Cu chelator *p*-SCN-Bz-DOTA (*p*-benzyl isothiocyanate-1,4,7,10-tetraazacyclododecane-1,4,7,10-tetraacetic acid. The resultant product was dextran-coated iron oxide nanoparticles label with ^{64}Cu. A representation of IONP-^{64}Cu nanoparticles for MRI and PET diagnosis is shown in Fig. 4. This nanosystem was nonspecifically taken up by macrophages. The study was carried out on Apo E$^{-/-}$ mice and the data suggested that the MR intensity signal decreased around the aortic valve due to the accumulation of iron oxide nanoparticles in the region. This effect was observed twenty-four hours after the injection of the nanoparticles.

Co-registration with PET signal confirms the accumulation in the region. Atherosclerotic human plaques have a few millimeters thick and length. PET, with its low resolution is unable to detect

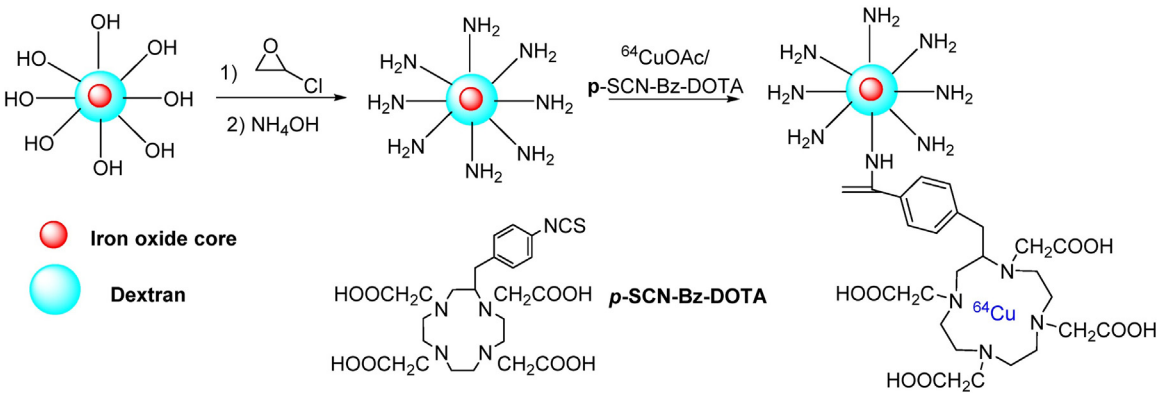

Fig. 4. Sequence of obtention IONP-^{64}Cu nanoparticles for MRI and PET diagnosis.

plaque structure. MRI has the resolution to map macrophages distribution in the plaques but lacks the sensitivity for screening. The combination of both techniques may complement to maximize the diagnostic potential of each one individually. Dextran-coated iron oxide nanoparticles were labeled with ^{64}Cu and treated with maleic anhydride to increase the negative surface charge to target the macrophage scavenger receptor (SR-A) [159]. The incorporation of ^{64}Cu was similar as described above. The acylation with maleic anhydride was performed using a borate buffer solution to keep the pH at 8,5 while the anhydride was slowly added. The radiolabeling of the final product, MDIO-^{64}Cu-DOTA, was 68%. Although maleate is not a specific ligand of the macrophage SR-A receptor, its suitable arrangement on the nanoparticle could result in a probe recognized and internalized by the SR-A receptor.

Nanoparticles for MRI and SPECT detection have also been recently addressed [160]. In this study USPIONs were synthesized by thermal decomposition of iron (III) acetylacetonate in diethylene glycol. In subsequent steps they were covered with aminated and carboxilated PEG and functionalized with DTPA for ^{99m}Tc coordination. The resulting nanoparticles were treated with Annexin V to target apoptotic macrophages in vulnerable plaques. This molecule recognizes the membrane lipid phosphatidylserine (PS), which is exposed on the surface cell when it dies. The contrast achieved in atherosclerotic plaques of Apo E$^{-/-}$ mice was adequate to identify them from normal tissues. A significant signal was detected after 5 h post-injection.

MRI-fluorescence systems have also been synthesized to evaluate vulnerable atherosclerotic plaques. Jaffer et al. added the near infrared fluorescent cyanine 5.5 to dextran-coated iron oxide nanoparticles. As described above, dextran was cross-linked with epichlorohydrin and aminated before the addition of the dye [161]. The final formulation presented 2.5 NIR fluorochromes per nanoparticle. Using a near infrared dye the autofluorescence from collagen, elastin and lipids components was minimized. Data arising from flow cytometry on activated macrophages, endothelial cells and smooth muscle cells incubated with the nanoparticles, revealed that the greatest uptake of the particles was registered on macrophages. In vivo studies were performed on Apo E$^{-/-}$ mice. A significant signal loss was observed in the aortic root and in the aortic arch after 24 h of 15 mg/kg of iron oxide injection. Evaluation under macroscopic light and near-infrared fluorescence (NIRF) confirmed the accumulation in aortic root and aortic arch. In a recent work, iron oxide nanoparticles were coated with meso-2,3-di*mer*captasuccinic acid (DMSA) and conjugated with the fluorescent dye NHS-Cy5.5 and with the polyclonal profiling-1 antibody, through the use of EDC and sulfo-NHS [162]. The overexpression of the protein profiling-1 is related to the development of cardiovascular diseases, including atherosclerosis, through the regulation of vascular smooth muscle cells (VSMCs) proliferation and migration. I*n vivo* fluorescence images revealed fluorescence signal in the carotid artery. This result was consistent with the MRI signal attenuation observed in a 9.4T MR imagining. These data were recovered after 36 h of the nanoparticles injection in Apo E$^{-/-}$ mice.

More recently, DMSA-coated MNPs were conjugated with Cy5.5 labeled osteopontin (ONP) antibody to target foamy macrophages [163]. The protein osteopontin is overexpressed in foamy macrophages in atherosclerotic lesions. The conjugation with the antibody was achieved through the amidation of the carboxylic group. The nanoparticles showed a hydrodynamic size of 92 nm and selectively accumulated in foamy macrophages. Such nanoparticles allowed the visualization of the atherosclerotic plaque by both MRI and a fluorescence imaging approach in a Apo E$^{-/-}$ mice model.

Song et al. prepared nanoagents for multimodal imaging (MRI and optical imaging) of microthrombous detection [164]. The formation of microthrombus occurs on the surface of vulnerable atherosclerotic plaques. Fibrin is a major component of thrombosis site, which makes it an interesting target to imaging unstable plaques. Aminated dextran-coated SPION were treated with the near-infrared dye IR787 and rhodamine-NHS.They were then modified with PEG and conjugated with the clot-binding peptide cysteine-arginine-glutamic acid-lysine-alanine (CREKA) in order to detect the formation of microthrombi by MRI. The CREKA-SPION with a hydrodynamic radius of about 100 nm, were assessed in terms of their ability to detect thrombus *in vitro* an in a rat model. It was very important the high density of CREKA molecules (around 2000 molecules) on the surface of SPION to detect fibrin in microthrombus.

Nahrendorf and co-workers developed a triple functional iron oxide nanoparticle to evaluate macrophages in atherosclerotic plaques. Dextran-coated iron oxide core was coupled with ^{64}Cu (using DTPA as chelator) and with the near-infrared fluorochrome Vivotag-680 [128]. The administrated doses to Apo E$^{-/-}$ mice were 1,5 mg/kg body weight. The final formulation combined the avidity of macrophages to take up dextran-iron oxide nanoparticles with the high sensitivity provided by the radiocenter; and the possibility of validation through fluorescence-based techniques. The three techniques confirmed the accumulation of nanoparticles in mouse atheroma.

Table 6 compares the different iron oxide based nanoparticles specifically modified to attain multimodal atherosclerosis diagnostic tools.

The development of multimodal diagnostic agents based on iron oxide nanoparticles is an emerging field and several nanoparticles have been designed to achieve this goal. Iron oxide magnetic nanoparticles for dual MRI and CT imaging were prepared although not intended for the detection of vulnerable

Table 6
Different iron oxide based nanoparticles specifically modified to attain multimodal atherosclerosis diagnostic tools.

Formulation	Coating	Incorporation of PET/NIRF label	Target	Targeting molecule	*In vivo*/*In vitro* assays	Ref.
MNP-^{64}Cu	Dextran	With Cu chelator *p*-SCN-Bz-DOTA	Macrophages	–	*In vivo*, in Apo E$^{-/-}$ mice	[158]
MNP-^{64}Cu	Dextran	With Cu chelator *p*-SCN-Bz-DOTA	Macrophages	Maleate, to target SR-A receptor	*In vitro*, using P388D1 murine macrophages	[159]
MNP-^{99m}Tc	PEG	With DTPA	Macrophages	Annexin V	*In vivo*, in Apo E$^{-/-}$ mice	[160]
MNP-Cy5.5	Dextran	Through amination of dextran	–	–	*In vivo*, in Apo E$^{-/--}$ mice	[161]
MNP-Cy5.5-PF$_1$	DMSA	Through conjugation reaction	Vascular smooth muscle cells	Profilin-1 antibody	*In vivo*, in Apo E$^{-/-}$ mice	[162]
MNP-CREKA-IR783	Dextran	Conjugation with the amine groups	Fibrin	CREKA	*In vivo*, in rat	[164]
MNP-^{64}Cu-Vivotag-680	Dextran	^{64}Cu with DTPA Vivotag-680 binding to the amines groups.	Macrophages	–	*In vivo*, in Apo E$^{-/-}$ mice	[128]
MNP-DMSA-Cy5.5-OPN	DMS	Amidation of carboxylic groups with EDC/sulfo-NHS	Foamy macrophages	Osteopontin	*In vivo*, in Apo E$^{-/-}$ mice	[163]

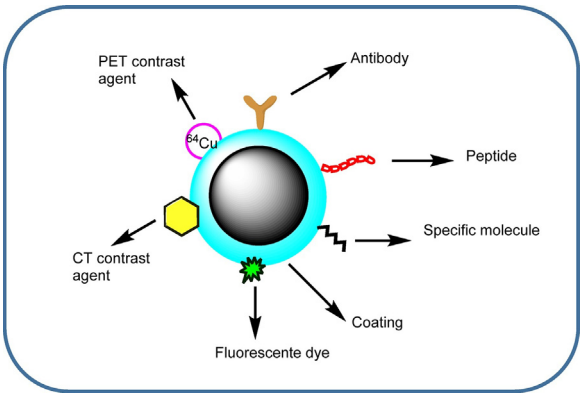

Fig. 5. Illustration of different MNPs modifiers to achieve multifunctional diagnostic tools.

atherosclerosis plaques. Lee et al. synthesized multifunctional Fe_3O_4/TaOx core/shell nanoparticles for tumor imaging [165]. Narayanan and co-workers synthesized magnetite/gold nanoparticles through a green chemistry procedure for MRI and CT imaging. In this case any particular pathology was focusing on [166].

Nanoparticles designed for MRI and PET represent a great attraction regarding to their application in atherosclerosis diagnosis, especially when a small molecule is used as targeting to reach specificity. Antibodies are frequently used as targeting. Besides their high cost, their use involves some drawbacks, such as the immunogenicity and that exhibit variations according to their source, affecting their efficiency as targeting ligands [167]. Fig. 5 shows all the possible modifications to active targeting atherosclerosis markers using MRI alone or in combination with other techniques.

Currently, many studies are focusing in the use of nanoparticles as theranostics agents, enabling the capabilities of diagnostic and therapy in a unique nanocarrier. Oumzil and co-workers synthesized solid lipid nanoparticles (SLN) charged with maghemite nanoparticles and the prostacyclin PGI2, which inhibits platelet aggregation. The nanoparticles showed excellent magnetic properties whereas the activity of PGI2 in the SLN was not affected [168]. Magnetic HDL-like nanostructure has been designed as a theranostic for atherosclerosis. Hydrophobic MNPs (coated with oleic acid) and hydrophilic MNPs (coated with citric acid) were charged into the HDL-like structure following different procedures. As a diagnostic tool the nanostructures showed higher magnetic resonance enhanced that the FDA-approved Ferumoxytol. The therapeutic effect of the HDL-like is based on the capability of the HDL to promote reverse cholesterol transport, leading to an atheroprotective effect [169]. The authors reported that the HDL-MNS induced higher cholesterol efflux than natural HDL [170].

6. Concluding remarks

Current knowledge of atherosclerosis reveals that the composition of the plaque appears as the main factor associated to the risk to suffer dramatic cardiovascular complications. Molecular imaging allows the detection of unstable plaques in a non-invasive way. Different techniques may be used to achieve this goal. Among them, MRI is one of the most extensively investigated. Among the most employed contrast agents for MRI, gadolinium and iron oxides are for far the most widely employed compounds. The use of gadolinium exhibits certain disadvantages mainly in patients with nephrotic diseases as well as in childs due to its nephrotoxicity. Therefore, iron oxide nanoparticles may be considered a reliable option.

Iron oxide nanoparticles are conveniently modified to target macrophages aiming to the earlier detection of vulnerable plaques. The reason is because macrophages are abundant in this kind of plaque and are present during all stages of atherosclerosis progression. Besides, more than one receptor overexpressed on activated macrophages may be distinguished; increasing the possibilities to functionalize nanoparticles with this purpose.

To overcome the limitations of MRI technique, iron oxide nanoparticles have been modified for multimodal diagnosis. Among the possible combinations, those nanoparticles for MRI/PET diagnosis seems to be the most studied for atherosclerosis, nowadays. This is associated to the synergic effect of this combination. The studies have been carried out using separating scanners for MRI and PET. The integration of these two techniques in a hybrid system involved a hard procedure to overcome serious difficulties [171].

Despite all the investigations about the use of iron oxide nanoparticles as contrast agents only a few formulations are currently available in the market and most of them are coated with dextran. The information recompiled in this review opens novel insight regarding to the specific target of MNP in order to obtain nanosystems able to increase the efficiency of the current diagnostic techniques. This contribution appears as a valuable tool faced not only in the design of novel contrast agents but also in the earlier and efficient detection of a wide gamma of chronical diseases among atherosclerosis [172].

Acknowledgments

The authors acknowledge the financial support of CONICET, ANPCyT (PICT 2013 1984) and UNS (PGI UNS 24-ZQ09). The collaboration of Mr. Giles from INOVA (S.A. Argentina) for the measurements in the clinical MR equipment. MGMS thanks to CONICET for the fellowship granted.

References

[1] P. Libby, The molecular mechanisms of the thrombotic complications of atherosclerosis, J. Lipid Res. 50 (2009) S352–S357, doi:http://dx.doi.org/10.1111/j.1365-2796.2008.01965.x.
[2] A.C. Van Der Wal, A.E. Becker, Atherosclerotic plaque rupture – pathologic basis of plaque stability and instability, Cardiovasc. Res. 41 (1999) 334–344, doi:http://dx.doi.org/10.1016/S0008-6363(98)00276-4.
[3] M.S. Ellulu, I. Patimah, H. Khaza'ai, A. Rahmat, Y. Abed, F. Ali, Atherosclerotic cardiovascular disease: a review of initiators and protective factors,

Inflammopharmacology 24 (2016) 1–10, doi:http://dx.doi.org/10.1007/s10787-015-0255-y.
[4] C. Silvestre-Roig, M.P. De Winther, C. Weber, M.J. Daemen, E. Lutgens, O. Soehnlein, Atherosclerotic plaque destabilization: mechanisms, models, and therapeutic strategies, Circ. Res. 114 (2014) 214–226, doi:http://dx.doi.org/10.1161/CIRCRESAHA.114.302355.
[5] K.J. Moore, I. Tabas, Macrophages in the pathogenesis of atherosclerosis, Cell 145 (2011) 341–355, doi:http://dx.doi.org/10.1016/j.cell.2011.04.005.
[6] J.F. Bentzon, F. Otsuka, R. Virmani, E. Falk, Mechanisms of plaque formation and rupture, Circ. Res. 114 (2014) 1852–1866, doi:http://dx.doi.org/10.1161/CIRCRESAHA.114.302721.
[7] S. Bozdağ Pehlivan, Nanotechnology-based drug delivery systems for targeting, imaging and diagnosis of neurodegenerative diseases, Pharm. Res. 30 (2013) 2499–2511, doi:http://dx.doi.org/10.1007/s11095-013-1156-7.
[8] S. Banyal, P. Malik, H.S. Tuli, T.K. Mukherjee, Advances in nanotechnology for diagnosis and treatment of tuberculosis, Curr. Opin. Pulm. Med. 19 (2013) 289–297, doi:http://dx.doi.org/10.1097/MCP.0b013e32835eff08.
[9] J. McCarroll, J. Teo, C. Boyer, D. Goldstein, M. Kavallaris, P.A. Phillips, Potential applications of nanotechnology for the diagnosis and treatment of pancreatic cancer, Front. Physiol. 5 (2014) 1–10, doi:http://dx.doi.org/10.3389/fphys.2014.00002.
[10] B. Godin, J.H. Sakamoto, R.E. Serda, A. Grattoni, A. Bouamrani, M. Ferrari, Emerging applications of nanomedicine for the diagnosis and treatment of cardiovascular diseases, Trends Pharmacol. Sci. 31 (2010) 199–205, doi:http://dx.doi.org/10.1016/j.tips.2010.01.003.
[11] A.H. Rezayan, M. Mosavi, S. Kheirjou, G. Amoabediny, M.S. Ardestani, J. Mohammadnejad, Monodisperse magnetite (Fe3O4) nanoparticles modified with water soluble polymers for the diagnosis of breast cancer by MRI method, J. Magn. Magn. Mater. 420 (2016) 210–217, doi:http://dx.doi.org/10.1016/j.jmmm.2016.07.003.
[12] Q.M. Kainz, O. Reiser, Reiser, scavengers, and reagents, Acc. Chem. Res. 47 (2014) 667–677.
[13] I.M.C. Lo Samuel, C.N. Tang, Magnetic nanoparticles: essential factors for sustainable\renvironmental applications, Water Res. 7 (2013) 2613–2632, doi:http://dx.doi.org/10.1016/j.watres.2013.02.039.
[14] I. Cicha, S. Lyer, C. Alexiou, C.D. Garlichs, Nanomedicine in diagnostics and therapy of cardiovascular diseases: beyond atherosclerotic plaque imaging, Nanotechnol. Rev. 2 (2013) 449–472, doi:http://dx.doi.org/10.1515/ntrev-2013-0009.
[15] F. Herranz, B. Salinas, H. Groult, J. Pellico, A. Lechuga-Vieco, R. Bhavesh, J. Ruiz-Cabello, Superparamagnetic nanoparticles for atherosclerosis imaging, Nanomaterials 4 (2014) 408–438, doi:http://dx.doi.org/10.3390/nano4020408.
[16] C. Gaurav, B. Saurav, R. Goutam, A.K. Goyal, Nano-systems for advanced therapeutics and diagnosis of atherosclerosis, Curr. Pharm. Des. (2015) 4498–4508.
[17] P. Padmanabhan, A. Kumar, S. Kumar, R.K. Chaudhary, B. Gulyás, Nanoparticles in practice for molecular-imaging applications: an overview, Acta Biomater. 41 (2016) 1–16, doi:http://dx.doi.org/10.1016/j.actbio.2016.06.003.
[18] P.G. Camici, O.E. Rimoldi, O. Gaemperli, P. Libby, Non-invasive anatomic and functional imaging of vascular inflammation and unstable plaque, Eur. Heart J. 33 (2012) 1309–1317, doi:http://dx.doi.org/10.1093/eurheartj/ehs067.
[19] M. Villien, H.-Y. Wey, J.B. Mandeville, C. Catana, J.R. Polimeni, C.Y. Sander, N.R. Zürcher, D.B. Chonde, J.S. Fowler, B.R. Rosen, J.M. Hooker, Dynamic functional imaging of brain glucose utilization using fPET-FDG, Neuroimage 100 (2014) 192–199, doi:http://dx.doi.org/10.1016/j.neuroimage.2014.06.025.
[20] M. Magnoni, E. Ammirati, P.G. Camici, Non-invasive molecular imaging of vulnerable atherosclerotic plaques, J. Cardiol. 65 (2015) 261–269, doi:http://dx.doi.org/10.1016/j.jjcc.2015.01.004.
[21] R. Weissleder, U. Mahmood, Molecular imaging 1, Radiology 219 (2001) 316–333.
[22] H. Herschman, Molecular imaging: looking at problems, Science 302 (80) (2003) 605–608.
[23] M. Phelps, Positron emission tomography provides molecular imaging of biological processes, Proc. Natl. Acad. Sci. 97 (2000) 9226–9233, doi:http://dx.doi.org/10.1073/pnas.97.16.9226.
[24] Y. Yang, Y. Sun, T. Cao, J. Peng, Y. Liu, Y. Wu, W. Feng, Y. Zhang, F. Li, Hydrothermal synthesis of NaLuF4:153Sm, Yb, Tm nanoparticles and their application in dual-modality upconversion luminescence and SPECT bioimaging, Biomaterials 34 (2013) 774–783, doi:http://dx.doi.org/10.1016/j.biomaterials.2012.10.022.
[25] M. Shilo, T. Reuveni, M. Motiei, R. Popovtzer, Nanoparticles as computed tomography contrast agents: current status and future perspectives, Nanomedicine 7 (2012) 257–269, doi:http://dx.doi.org/10.2217/nnm.11.190.
[26] Nicolas Ducros, Andrea Bassi, Gianluca Valentini, Gianfranco Canti, Simon Arridge, Cosimo D'Andrea, Fluorescence molecular tomography of an animal model using structured light rotating view acquisition, J. Biomed. Opt. 18 (2013) 20503, doi:http://dx.doi.org/10.1117/1.JBO.18.2.020503.
[27] L. Nie, X. Chen, Structural and functional photoacoustic molecular tomography aided by emerging contrast agents, Chem. Soc. Rev. 43 (2014) 7132–7170, doi:http://dx.doi.org/10.1039/c4cs00086b.
[28] L.V. Wang, S. Hu, Photoacoustic tomography In vivo imaging from organelles to organs, Science 335 (80) (2012) 1458–1462, doi:http://dx.doi.org/10.1126/science.1216210.
[29] J. Huang, X. Zhong, L. Wang, L. Yang, H. Mao, Improving the magnetic resonance imaging contrast and detection methods with engineered magnetic nanoparticles, Theranostics 2 (2012) 86–102, doi:http://dx.doi.org/10.7150/thno.4006.
[30] J. Li, J. Zhu, Quantum dots for fluorescent biosensing and bio-imaging applications, Analyst 138 (2013) 2506–2515, doi:http://dx.doi.org/10.1039/c3an36705c.
[31] C. Peng, L. Zheng, Q. Chen, M. Shen, R. Guo, H. Wang, X. Cao, G. Zhang, X. Shi, Biomaterials PEGylated dendrimer-entrapped gold nanoparticles for in vivo blood pool and tumor imaging by computed tomography, Biomaterials 33 (2012), doi:http://dx.doi.org/10.1016/j.biomaterials.2011.10.052.
[32] N. Lee, T. Hyeon, Designed synthesis of uniformly sized iron oxide nanoparticles for efficient magnetic resonance imaging contrast agents, Chem. Soc. Rev. 41 (2012) 2575–2589, doi:http://dx.doi.org/10.1039/C1CS15248C.
[33] R. Tietze, S. Lyer, S. Dürr, T. Struffert, T. Engelhorn, M. Schwarz, E. Eckert, T. Göen, S. Vasylyev, W. Peukert, F. Wiekhorst, L. Trahms, A. Dörfler, C. Alexiou, Efficient drug-delivery using magnetic nanoparticles—biodistribution and therapeutic effects in tumour bearing rabbits, Nanomed. Nanotechnol. Biol. Med. 9 (2013) 961–971, doi:http://dx.doi.org/10.1016/j.nano.2013.05.001.
[34] V.V. Mody, A. Cox, S. Shah, A. Singh, W. Bevins, H. Parihar, Magnetic nanoparticle drug delivery systems for targeting tumor, Appl. Nanosci. 4 (2014) 385–392, doi:http://dx.doi.org/10.1007/s13204-013-0216-y.
[35] A. Ranzoni, G. Sabatte, L.J. Van Ijzendoorn, M.W.J. Prins, One-step homogeneous magnetic nanoparticle immunoassay for biomarker detection directly in blood plasma, ACS Nano 6 (2012) 3134–3141, doi:http://dx.doi.org/10.1021/nn204913f.
[36] M.F. Horst, D.F. Coral, M.B. Fernández van Raap, M. Alvarez, V. Lassalle, Hybrid nanomaterials based on gum Arabic and magnetite for hyperthermia treatments, Mater. Sci. Eng. C 74 (2016) 443–450, doi:http://dx.doi.org/10.1016/j.msec.2016.12.035.
[37] M. Muñoz de Escalona, E. Sáez-Fernández, J.C. Prados, C. Melguizo, J.L. Arias, Magnetic solid lipid nanoparticles in hyperthermia against colon cancer, Int. J. Pharm. 504 (2016) 11–19, doi:http://dx.doi.org/10.1016/j.ijpharm.2016.03.005.
[38] M. Calero, L. Gutiérrez, G. Salas, Y. Luengo, A. Lázaro, P. Acedo, M.P. Morales, R. Miranda, A. Villanueva, Efficient and safe internalization of magnetic iron oxide nanoparticles: two fundamental requirements for biomedical applications, Nanomed. Nanotechnol. Biol. Med. 10 (2014) 733–743, doi:http://dx.doi.org/10.1016/j.nano.2013.11.010.
[39] W. Wu, Z. Wu, T. Yu, C. Jiang, W.-S. Kim, Recent progress on magnetic iron oxide nanoparticles: synthesis, surface functional strategies and biomedical applications, Sci. Technol. Adv. Mater. 16 (2015) 23501, doi:http://dx.doi.org/10.1088/1468-6996/16/2/023501.
[40] J. Estelrich, M.J. Sánchez-Martín, M.A. Busquets, Nanoparticles in magnetic resonance imaging: from simple to dual contrast agents, Int. J. Nanomed. 10 (2015) 1727–1741, doi:http://dx.doi.org/10.2147/IJN.S76501.
[41] H.S. Thomsen, Nephrogenic systemic fibrosis: a serious adverse reaction to gadolinium – 1997–2006–2016. Part 1, Acta Radiol. 57 (2016) 515–520, doi:http://dx.doi.org/10.1177/0284185115626480.
[42] A.K. Abu-Alfa, Nephrogenic systemic fibrosis and gadolinium-Based contrast agents, Adv. Chron. Kidney Dis. 18 (2011) 188–198, doi:http://dx.doi.org/10.1053/j.ackd.2011.03.001.
[43] K. Nwe, M. Bernardo, C.A.S. Regino, M. Williams, M.W. Brechbiel, Comparison of MRI properties between derivatized DTPA and DOTA gadolinium-dendrimer conjugates, Bioorg. Med. Chem. 18 (2010) 5925–5931, doi:http://dx.doi.org/10.1016/j.bmc.2010.06.086.
[44] T. Kanda, T. Fukusato, M. Matsuda, K. Toyoda, H. Oba, J. Kotoku, T. Haruyama, K. Kitajima, S. Furui, Gadolinium-based contrast agent accumulates in the brain even in subjects without severe renal dysfunction: evaluation of autopsy brain specimens with inductively coupled plasma mass spectroscopy, Radiology 276 (2015) 228–232, doi:http://dx.doi.org/10.1148/radiol.2015142690.
[45] N. Murata, L.F. Gonzalez-Cuyar, K. Murata, C. Fligner, R. Dills, D. Hippe, K.R. Maravilla, Macrocyclic and other non–group 1 gadolinium contrast agents deposit low levels of gadolinium in brain and bone tissue, Invest. Radiol. 51 (2016) 447–453, doi:http://dx.doi.org/10.1097/RLI.0000000000000252.
[46] M. Rogosnitzky, S. Branch, Gadolinium-based contrast agent toxicity: a review of known and proposed mechanisms, Biometals 29 (2016) 365–376, doi:http://dx.doi.org/10.1007/s10534-016-9931-7.
[47] R. Chen, D. Ling, L. Zhao, S. Wang, Y. Liu, R. Bai, S. Baik, Y. Zhao, C. Chen, T. Hyeon, Parallel comparative studies on mouse toxicity of oxide nanoparticle- and gadolinium-based T1 MRI contrast agents, ACS Nano 9 (2015) 12425–12435, doi:http://dx.doi.org/10.1021/acsnano.5b05783.
[48] R.F. Reilly, Risk for nephrogenic systemic fibrosis with gadoteridol (ProHance) in patients who are on long-term hemodialysis, Clin. J. Am. Soc Nephrol. 3 (2008) 747–751, doi:http://dx.doi.org/10.2215/CJN.05721207.
[49] A. Szpak, S. Fiejdasz, W. Prendota, T. Strączek, C. Kapusta, J. Szmyd, M. Nowakowska, S. Zapotoczny, T1-T2 Dual-modal MRI contrast agents based on superparamagnetic iron oxide nanoparticles with surface attached gadolinium complexes, J. Nanopar. Res. 16 (2014) 2678, doi:http://dx.doi.org/10.1007/s11051-014-2678-6.
[50] M. Yang, L. Gao, K. Liu, C. Luo, Y. Wang, Talanta nanoparticles as T1 and T2 dual mode MRI contrast agent, Talanta 131 (2015) 661–665, doi:http://dx.doi.org/10.1016/j.talanta.2014.08.042.

[51] H. Jung, B. Park, C. Lee, J. Cho, J. Suh, J. Park, Y. Kim, J. Kim, G. Cho, H. Cho, Dual MRI t 1 and t 2 (*) contrast with size-controlled iron oxide nanoparticles, Nanomed. Nanotechnol. Biol. Med. 10 (2014) 1679–1689, doi:http://dx.doi.org/10.1016/j.nano.2014.05.003.
[52] T. Christen, W. Ni, D. Qiu, H. Schmiedeskamp, R. Bammer, M. Moseley, G. Zaharchuk, High-resolution cerebral blood volume imaging in humans using the blood pool contrast agent ferumoxytol, Magn. Reson. Med. 70 (2013) 705–710, doi:http://dx.doi.org/10.1002/mrm.24500.
[53] B. Turkbey, H.K. Agarwal, J. Shih, M. Bernardo, Y.L. McKinney, D. Daar, G.L. Griffiths, S. Sankineni, L. Johnson, K.B. Grant, J. Weaver, S. Rais-Bahrami, M. Harisinghani, P. Jacobs, W. Dahut, M.J. Merino, P.A. Pinto, P.L. Choyke, A phase I dosing study of ferumoxytol for MR lymphography at 3 T in patients with prostate cancer, Am. J. Roentgenol. 205 (2015) 64–69, doi:http://dx.doi.org/10.2214/AJR.14.13009.
[54] T. Yokoo, T. Wolfson, K. Iwaisako, M.R. Peterson, H. Mani, Z. Goodman, C. Changchien, M.S. Middleton, A.C. Gamst, S.M. Mazhar, Y. Kono, S.B. Ho, C.B. Sirlin, Evaluation of liver fibrosis using texture analysis on combined-contrast-enhanced magnetic resonance images at 3. 0T, BioMed. Res. Int. 2015 (2015), doi:http://dx.doi.org/10.1155/2015/387653.
[55] S. Maurea, P.P. Mainenti, A. Tambasco, M. Imbriaco, C. Mollica, E. Laccetti, L. Camera, R. Liuzzi, M. Salvatore, Diagnostic accuracy of MR imaging to identify and characterize focal liver lesions: comparison between gadolinium and superparamagnetic iron oxide contrast media, Quant. Imaging Med. Surg. 4 (2014) 181–189, doi:http://dx.doi.org/10.3978/j.issn.2223-4292.2014.01.02.
[56] P. Mosler, F. Akisik, K. Sandrasegaran, E. Fogel, J. Watkins, W. Alazmi, S. Sherman, G. Lehman, T. Imperiale, L. McHenry, Accuracy of magnetic resonance cholangiopancreatography in the diagnosis of pancreas divisum, Dig. Dis. Sci. 57 (2012) 170–174, doi:http://dx.doi.org/10.1007/s10620-011-1823-7.
[57] A.S. Fortuin, R. Brüggemann, J. van der Linden, I. Panfilov, B. Israël, T.W.J. Scheenen, J.O. Barentsz, Ultra-small superparamagnetic iron oxides for metastatic lymph node detection: back on the block, Wiley Interdiscip. Rev. Nanomed. Nanobiotechnol. (2017) e1471, doi:http://dx.doi.org/10.1002/wnan.1471.
[58] W. Liu, L. Nie, F. Li, Z.P. Aguilar, H. Xu, Y. Xiong, F. Fu, H. Xu, Folic acid conjugated magnetic iron oxide nanoparticles for nondestructive separation and detection of ovarian cancer cells from whole blood, Biomater. Sci. 4 (2016) 159–166, doi:http://dx.doi.org/10.1039/C5BM00207A.
[59] M.K.G. Lima-Tenório, E.A. Pineda, N.M. Ahmad, H. Fessi, A. Elaissari, Magnetic nanoparticles: in vivo cancer diagnosis and therapy, Int. J. Pharm. 493 (2015) 313–327, doi:http://dx.doi.org/10.1016/j.ijpharm.2015.07.059.
[60] I. Rosenberger, A. Strauss, S. Dobiasch, C. Weis, S. Szanyi, L. Gil-Iceta, E. Alonso, M. González Esparza, V. Gómez-Vallejo, B. Szczupak, S. Plaza-García, S. Mirzaei, L.L. Israel, S. Bianchessi, E. Scanziani, J.P. Lellouche, P. Knoll, J. Werner, K. Felix, L. Grenacher, T. Reese, J. Kreuter, M. Jiménez-González, Targeted diagnostic magnetic nanoparticles for medical imaging of pancreatic cancer, J. Control. Release 214 (2015) 76–84, doi:http://dx.doi.org/10.1016/j.jconrel.2015.07.017.
[61] V.L. Lassalle, M. Avena, M.L. Ferreira, A review of the methods of magnetic nanocomposites synthesis and their applications as drug delivery systems and immobilization supports for lipases, Curr. Trends Polym. Sci. 1 (2006).
[62] S.F. Hasany, I. Ahmed, R.J.A. Rehman, Systematic review of the preparation techniques of iron oxide magnetic nanoparticles, Nanosci. Nanotechnol. 2 (2012) 148–158, doi:http://dx.doi.org/10.5923/j.nn.20120206.01.
[63] A.R. Nochehdehi, S. Thomas, M. Sadri, S.S.S. Afghahi, S.M. Mehdi Hadavi, Iron oxide biomagnetic nanoparticles (IO-BMNPs); synthesis, characterization and biomedical application – a review, J. Nanomed. Nanotechnol. 8 (2017) 2, doi:http://dx.doi.org/10.4172/2157-7439.1000423.
[64] L.H. Reddy, J.L. Arias, J. Nicolas, P. Couvreur, Magnetic nanoparticles: design and characerization, toxicity and biocompatibility, Pharm. Biomed. Appl. Chem. Rev. 112 (2012) 5818–5878, doi:http://dx.doi.org/10.1021/cr300068p.
[65] E. Tombácz, R. Turcu, V. Socoliuc, L. Vékás, Magnetic iron oxide nanoparticles: recent trends in design and synthesis of magnetoresponsive nanosystems, Biochem. Biophys. Res. Commun. 468 (2015) 442–453, doi:http://dx.doi.org/10.1016/j.bbrc.2015.08.030.
[66] P. Azcona, R. Zysler, V. Lassalle, Simple and novel strategies to achieve shape and size control of magnetite nanoparticles intended for biomedical applications, Colloids Surf. A Physicochem. Eng. Asp. 504 (2016) 320–330, doi:http://dx.doi.org/10.1016/j.colsurfa.2016.05.064.
[67] L.K. Petersen, A.W. York, D.R. Lewis, S. Ahuja, K.E. Uhrich, R.K. Prudhomme, P. V. Moghe, Amphiphilic nanoparticles repress macrophage atherogenesis: novel core/shell designs for scavenger receptor targeting and down-regulation, Mol. Pharm. 11 (2014) 2815–2824, doi:http://dx.doi.org/10.1021/mp500188g.
[68] M.C. Mascolo, Y. Pei, T.A. Ring, Room temperature co-precipitation synthesis of magnetite nanoparticles in a large ph window with different bases, Materials (Basel) 6 (2013) 5549–5567, doi:http://dx.doi.org/10.3390/ma6125549.
[69] P. Nicolás, M. Saleta, H. Troiani, R. Zysler, V. Lassalle, M.L. Ferreira, Preparation of iron oxide nanoparticles stabilized with biomolecules: experimental and mechanistic issues, Acta Biomater. 9 (2013) 4754–4762, doi:http://dx.doi.org/10.1016/j.actbio.2012.09.040.
[70] R. Valenzuela, M.C. Fuentes, C. Parra, J. Baeza, N. Duran, S.K. Sharma, M. Knobel, J. Freer, Influence of stirring velocity on the synthesis of magnetite nanoparticles (Fe3O4) by the co-precipitation method, J. Alloys Compd. 488 (2009) 227–231, doi:http://dx.doi.org/10.1016/j.jallcom.2009.08.087.
[71] S. Ge, X. Shi, K. Sun, C. Li, J.R. Baker, M.M. Banaszak Holl, B.G. Orr, A facile hydrothermal synthesis of iron oxide nanoparticles with tunable magnetic properties, J. Phys. Chem. C Nanomater. Interfaces 113 (2009) 13593–13599, doi:http://dx.doi.org/10.1021/jp902953t.
[72] J. Yan, S. Mo, J. Nie, W. Chen, X. Shen, J. Hu, G. Hao, H. Tong, Hydrothermal synthesis of monodisperse Fe3O4 nanoparticles based on modulation of tartaric acid, Colloids Surf. A Physicochem. Eng. Asp. 340 (2009) 109–114, doi:http://dx.doi.org/10.1016/j.colsurfa.2009.03.016.
[73] C.Y. Haw, F. Mohamed, C.H. Chia, S. Radiman, S. Zakaria, N.M. Huang, H.N. Lim, Hydrothermal synthesis of magnetite nanoparticles as MRI contrast agents, Ceram. Int. 36 (2010) 1417–1422, doi:http://dx.doi.org/10.1016/j.ceramint.2010.02.005.
[74] K. Woo, J. Hong, S. Choi, H.-W. Lee, J. Ahn, C.S. Kim, S.W. Lee, Easy synthesis and magnetic properties of iron oxide nanoparticles, Chem. Mater. 16 (2004) 2814–2818, doi:http://dx.doi.org/10.1021/cm049552x.
[75] T.K.O. Vuong, D.L. Tran, T.L. Le, D.V. Pham, H.N. Pham, T.H.L. Ngo, H.M. Do, X.P. Nguyen, Synthesis of high-magnetization and monodisperse Fe3O4 nanoparticles via thermal decomposition, Mater. Chem. Phys. 163 (2015) 537–544, doi:http://dx.doi.org/10.1016/j.matchemphys.2015.08.010.
[76] V. Patsula, L. Kosinová, M. Lovrić, L. Ferhatovic Hamzić, M. Rabyk, R. Konefal, A. Paruzel, M. Šlouf, V. Herynek, S. Gajović, D. Horák, Superparamagnetic Fe 3 O 4 nanoparticles: synthesis by thermal decomposition of Iron(III) glucuronate and application in magnetic resonance imaging3, Colloids Surf. A Physicochem. Mater. Interfaces 8 (2016) 7238–7247, doi:http://dx.doi.org/10.1021/acsami.5b12720.
[77] C.H.W. Kelly, M. Lein, Choosing the right precursor for thermal decomposition solution-phase synthesis of iron nanoparticles: tunable dissociation energies of ferrocene derivatives, Phys. Chem. Chem. Phys. 18 (2016) 32448–32457, doi:http://dx.doi.org/10.1039/C6CP06921E.
[78] F.B. Effenberger, R.A. Couto, P.K. Kiyohara, G. Machado, S.H. Masunaga, R.F. Jardim, L.M. Rossi, Economically attractive route for the preparation of high quality magnetic nanoparticles by the thermal decomposition of iron(III) acetylacetonate, Nanotechnology 28 (2017) 115603, doi:http://dx.doi.org/10.1088/1361-6528/aa5ab0.
[79] J. Xu, H. Yang, W. Fu, K. Du, Y. Sui, J. Chen, Y. Zeng, M. Li, G. Zou, Preparation and magnetic properties of magnetite nanoparticles by sol-gel method, J. Magn. Magn. Mater. 309 (2007) 307–311, doi:http://dx.doi.org/10.1016/j.jmmm.2006.07.037.
[80] S. Shaker, S. Zafarian, C. Chakra Shilpa, K.V. Rao, Preparation and characterization of magnetite nanoparticles by sol-gel method, Int. J. Innov. Res. Sci. Eng. Technol. 2 (2013) 2969–2973, doi:http://dx.doi.org/10.4028/www.scientific.net/AMM.618.24.
[81] O.M. Lemine, K. Omri, B. Zhang, L. El Mir, M. Sajieddine, A. Alyamani, M. Bououdina, Sol-gel synthesis of 8 nm magnetite (Fe3O4) nanoparticles and their magnetic properties, Superlattices Microstruct. 52 (2012) 793–799, doi:http://dx.doi.org/10.1016/j.spmi.2012.07.009.
[82] K.S. Suslick, Sonochemistry, Science 247 (1990) 1439–1445, doi:http://dx.doi.org/10.1126/science.247.4949.1439.
[83] F. Dang, N. Enomoto, J. Hojo, K. Enpuku, Sonochemical synthesis of monodispersed magnetite nanoparticles by using an ethanol-water mixed solvent, Ultrason. Sonochem. 16 (2009) 649–654, doi:http://dx.doi.org/10.1016/j.ultsonch.2008.11.003.
[84] G. Marchegiani, P. Imperatori, A. Mari, L. Pilloni, A. Chiolerio, P. Allia, P. Tiberto, L. Suber, Sonochemical synthesis of versatile hydrophilic magnetite nanoparticles, Ultrason. Sonochem. 19 (2012) 877–882, doi:http://dx.doi.org/10.1016/j.ultsonch.2011.12.007.
[85] V. Sreeja, P.A. Joy, Microwave-hydrothermal synthesis of γ-Fe2O3 nanoparticles and their magnetic properties, Mater. Res. Bull. 42 (2007) 1570–1576, doi:http://dx.doi.org/10.1016/j.materresbull.2006.11.014.
[86] W.W. Wang, Y.J. Zhu, M.L. Ruan, Microwave-assisted synthesis and magnetic property of magnetite and hematite nanoparticles, J. Nanopart. Res. 9 (2007) 419–426, doi:http://dx.doi.org/10.1007/s11051-005-9051-8.
[87] T. Caillot, D. Aymes, D. Stuerga, N. Viart, G. Pourroy, Microwave flash synthesis of iron and magnetite particles by disproportionation of ferrous alcoholic solutions, J. Mater. Sci. 37 (2002) 5153–5158, doi:http://dx.doi.org/10.1023/A:1021028809382.
[88] W.-W. Wang, Y.-J. Zhu, Microwave-assisted synthesis of magnetite nanosheets in mixed solvents of ethylene glycol and water, Curr. Nanosci. 3 (2007) 171–176, doi:http://dx.doi.org/10.2174/157341307780619233.
[89] T. Schneider, A. Löwa, S. Karagiozov, L. Sprenger, L. Gutiérrez, T. Esposito, G. Marten, K. Saatchi, U.O. Häfeli, Facile microwave synthesis of uniform magnetic nanoparticles with minimal sample processing, J. Magn. Magn. Mater. 421 (2017) 283–291, doi:http://dx.doi.org/10.1016/j.jmmm.2016.07.063.
[90] M.J. Williams, E. Sánchez, E. Aluri, F. Douglas, D.A. Maclaren, O. Collins, E. Cussen, J. Budge, L. Saunders, M. Michaelis, M. Smales, J. Cinatl Jr., S. Lorrio Gonzalez, D. Kruger, R.T.M. de Rosales, S. Corr, Microwave-assisted syntheis of highly crystalline, multifunctional iron oxide nanocomposites for imaging applications, RSC Adv. 6 (2016) 83520–83528, doi:http://dx.doi.org/10.1039/C6RA11819D.
[91] S. Bano, S. Nazir, A. Nazir, S. Munir, T. Mahmood, M. Afzal, F.L. Ansari, K. Mazhar, Microwave-assisted green synthesis of superparamagnetic nanoparticles using fruit peel extracts: surface engineering, T2relaxometry, and photodynamic treatment potential, Int. J. Nanomed. 11 (2016) 3833–3848, doi:http://dx.doi.org/10.2147/IJN.S106553.

[92] W.S. Peternele, V. Monge Fuentes, M.L. Fascineli, J. Rodrigues Da Silva, R.C. Silva, C.M. Lucci, R. Bentes De Azevedo, Experimental investigation of the coprecipitation method: an approach to obtain magnetite and maghemite nanoparticles with improved properties, J. Nanomater. 2014 (2014) 1–10, doi:http://dx.doi.org/10.1155/2014/682985.
[93] S. Theerdhala, D. Bahadur, S. Vitta, N. Perkas, Z. Zhong, A. Gedanken, Sonochemical stabilization of ultrafine colloidal biocompatible magnetite nanoparticles using amino acid, l-arginine, for possible bio applications, Ultrason. Sonochem. 17 (2010) 730–737, doi:http://dx.doi.org/10.1016/j.ultsonch.2009.12.007.
[94] I.V. Kubrakova, I.Y. Koshcheeva, D.V. Pryazhnikov, L.Y. Martynov, M.S. Kiseleva, O.A. Tyutyunnik, Microwave synthesis, properties and analytical possibilities of magnetite-based nanoscale sorption materials, J. Anal. Chem. 69 (2014) 336–346, doi:http://dx.doi.org/10.1134/S1061934814020087.
[95] B.M. Kumfer, K. Shinoda, B. Jeyadevan, I.M. Kennedy, Gas-phase flame synthesis and properties of magnetic iron oxide nanoparticles with reduced oxidation state, J. Aerosol Sci. 41 (2010) 257–265, doi:http://dx.doi.org/10.1016/j.jaerosci.2010.01.003.
[96] F. Fajaroh, H. Setyawan, W. Widiyastuti, S. Winardi, Synthesis of magnetite nanoparticles by surfactant-free electrochemical method in an aqueous system, Adv. Powder Technol. 23 (2012) 328–333, doi:http://dx.doi.org/10.1016/j.apt.2011.04.007.
[97] M. Darbandi, F. Stromberg, J. Landers, N. Reckers, B. Sanyal, W. Keune, H. Wende, Nanoscale size effect on surface spin canting in iron oxide nanoparticles synthesized by the microemulsion method, J. Phys. D Appl. Phys. 45 (2012) 195001, doi:http://dx.doi.org/10.1088/0022-3727/45/19/195001.
[98] J.D. Obayemi, S. Dozie-Nwachukwu, Y. Danyuo, O.S. Odusanya, N. Anuku, K. Malatesta, W.O. Soboyejo, Biosynthesis and the conjugation of magnetite nanoparticles with luteinizing hormone releasing hormone (LHRH), Mater. Sci. Eng. C 46 (2015) 482–496, doi:http://dx.doi.org/10.1016/j.msec.2014.10.081.
[99] P.A. Sundaram, R. Augustine, M. Kannan, Extracellular biosynthesis of iron oxide nanoparticles by Bacillus subtilis strains isolated from rhizosphere soil, Biotechnol. Bioprocess Eng. 17 (2012) 835–840, doi:http://dx.doi.org/10.1007/s12257-011-0582-9.
[100] R. Jin, B. Lin, D. Li, H. Ai, Superparamagnetic iron oxide nanoparticles for MR imaging and therapy: design considerations and clinical applications, Curr. Opin. Pharmacol. 18 (2014) 18–27, doi:http://dx.doi.org/10.1016/j.coph.2014.08.002.
[101] H. Wang, T. Camilla, L. Xiaowen, K. Bridle, G. Jeffrey, Y. Zhu, D. Crawford, Z. Xu, X. Liu, R. Michael, Diagnostic imaging and therapeutic application of nanoparticles targeting to the liver, J. Mater. Chem. B 3 (2015) 939–958, doi:http://dx.doi.org/10.1039/b000000x.
[102] M. Di Marco, C. Sadun, M. Port, I. Guilbert, P. Couvreur, C. Dubernet, Physicochemical characterization of ultrasmall superparamagnetic iron oxide nanoparticles for biomedical application as MRI contrast agents, Int. J. Nanomed. 2 (2007) 609–622. http://www.dovepress.com/getfile.php?fileID=1949.
[103] K. Turcheniuk, A.V. Tarasevych, V.P. Kukhar, R. Boukherroub, S. Szunerits, Recent advances in surface chemistry strategies for the fabrication of functional iron oxide based magnetic nanoparticles, Nanoscale 5 (2013) 10729–10752, doi:http://dx.doi.org/10.1039/c3nr04131j.
[104] M. Muthiah, I. Park, C. Cho, Surface modi fi cation of iron oxide nanoparticles by biocompatible polymers for tissue imaging and targeting, Biotechnol. Adv. 31 (2013) 1224–1236, doi:http://dx.doi.org/10.1016/j.biotechadv.2013.03.005.
[105] J. Xie, C. Xu, N. Kohler, Y. Hou, S. Sun, Controlled PEGylation of monodisperse Fe3O4 nanoparticles for reduced non-specific uptake by macrophage cells, Adv. Mater. 19 (2007) 3163–3166, doi:http://dx.doi.org/10.1002/adma.200701975.
[106] R.Y. Hong, B. Feng, L.L. Chen, G.H. Liu, H.Z. Li, Y. Zheng, D.G. Wei, Synthesis, characterization and MRI application of dextran-coated Fe3O4 magnetic nanoparticles, Biochem. Eng. J. 42 (2008) 290–300, doi:http://dx.doi.org/10.1016/j.bej.2008.07.009.
[107] G. Liu, R.Y. Hong, L. Guo, Y.G. Li, H.Z. Li, Preparation, characterization and MRI application of carboxymethyl dextran coated magnetic nanoparticles, Appl. Surf. Sci. 257 (2011) 6711–6717, doi:http://dx.doi.org/10.1016/j.apsusc.2011.02.110.
[108] V. Zamora-Mora, M. Fernández-Gutiérrez, J.S. Román, G. Goya, R. Hernández, C. Mijangos, Magnetic core–shell chitosan nanoparticles: rheological characterization and hyperthermia application, Carbohydr. Polym. 102 (2014) 691–698, doi:http://dx.doi.org/10.1016/j.carbpol.2013.10.101.
[109] P.B. Shete, R.M. Patil, N.D. Thorat, A. Prasad, R.S. Ningthoujam, S.J. Ghosh, S.H. Pawar, Magnetic chitosan nanocomposite for hyperthermia therapy application: preparation, characterization and in vitro experiments, Appl. Surf. Sci. 288 (2014) 149–157, doi:http://dx.doi.org/10.1016/j.apsusc.2013.09.169.
[110] M. Agotegaray, S. Palma, V. Lassalle, Novel chitosan coated magnetic nanocarriers for the targeted diclofenac delivery, J. Nanosci. Nanotechnol. 14 (2014) 3343–3347, doi:http://dx.doi.org/10.1166/jnn.2014.8256.
[111] S.M.- Samani, R. Miri, M. Salmanpour, N. Khalighian, S. Sotoudeh, N. Erfani, Preparation and assessment of chitosan- coated superparamagnetic Fe 3 O 4 nanoparticles for controlled delivery of methotrexate, Res. Pharm. Sci. 8 (2014) 25–33.
[112] X.N. Pham, T.P. Nguyen, T.N. Pham, T.T.N. Tran, T.V.T. Tran, Synthesis and characterization of chitosan-coated magnetite nanoparticles and their application in curcumin drug delivery, Adv. Nat. Sci. Nanosci. Nanotechnol. 7 (2016) 45010, doi:http://dx.doi.org/10.1088/2043-6262/7/4/045010.
[113] A. Ruiz, Y. Hernández, C. Cabal, E. González, S. Veintemillas-Verdaguer, E. Martínez, M.P. Morales, Biodistribution and pharmacokinetics of uniform magnetite nanoparticles chemically modified with polyethylene glycol, Nanoscale 5 (2013) 11400, doi:http://dx.doi.org/10.1039/c3nr01412f.
[114] M. Wagner, S. Wagner, J. Schnorr, E. Schellenberger, D. Kivelitz, L. Krug, M. Dewey, M. Laule, B. Hamm, M. Taupitz, Coronary MR angiography using citrate-coated very small superparamagnetic iron oxide particles as blood-pool contrast agent: initial experience in humans, J. Magn. Reson. Imaging 34 (2011) 816–823, doi:http://dx.doi.org/10.1002/jmri.22683.
[115] S. Srivastava, R. Awasthi, N.S. Gajbhiye, V. Agarwal, A. Singh, A. Yadav, R.K. Gupta, Innovative synthesis of citrate-coated superparamagnetic Fe3O4 nanoparticles and its preliminary applications, J. Colloid Interface Sci. 359 (2011) 104–111, doi:http://dx.doi.org/10.1016/j.jcis.2011.03.059.
[116] M.E. de Sousa, M.B. Fernández van Raap, P.C. Rivas, P. Mendoza Zélis, P. Girardin, G.A. Pasquevich, J.L. Alessandrini, D. Muraca, F.H. Sánchez, Stability and relaxation mechanisms of citric acid coated magnetite nanoparticles for magnetic hyperthermia, J. Phys. Chem. C 117 (2013) 5436–5445, doi:http://dx.doi.org/10.1021/jp311556b.
[117] E. Cheraghipour, S. Javadpour, A.R. Mehdizadeh, Citrate capped superparamagnetic iron oxide nanoparticles used for hyperthermia therapy, J. Biomed. Sci. Eng. 5 (2012) 715–719, doi:http://dx.doi.org/10.4236/jbise.2012.512089.
[118] V. Sreeja, K.N. Jayaprabha, P.A. Joy, Water-dispersible ascorbic-acid-coated magnetite nanoparticles for contrast enhancement in MRI, Appl. Nanosci. 5 (2015) 435–441, doi:http://dx.doi.org/10.1007/s13204-014-0335-0.
[119] L. Xiao, J. Li, D.F. Brougham, E.K. Fox, N. Feliu, A. Bushmelev, N. Mertens, F. Kiessling, M. Valldor, B. Fadeel, S. Mathur, Water-soluble superparamagnetic magnetite nanoparticles with biocompatible coating for enhanced magnetic resonance imaging (MRI) water-soluble superparamagnetic magnetite nanoparticles with biocompatible coating for enhanced magnetic resonance imaging, ACS Nano (2011) 6315–6324, doi:http://dx.doi.org/10.1021/nn201348s.
[120] P.I.P. Soares, C.A.T. Laia, A. Carvalho, L.C.J. Pereira, J.T. Coutinho, I.M.M. Ferreira, C.M.M. Novo, J.P. Borges, Iron oxide nanoparticles stabilized with a bilayer of oleic acid for magnetic hyperthermia and MRI applications, Appl. Surf. Sci. 383 (2016) 240–247, doi:http://dx.doi.org/10.1016/j.apsusc.2016.04.181.
[121] S. Moraes Silva, R. Tavallaie, L. Sandiford, R. Tilley, J.J. Gooding, Gold coated magnetic nanoparticles: preparation, surface modification for analytical and biomedical applications, Chem. Commun. 52 (2016) 7528–7540, doi:http://dx.doi.org/10.1039/C6CC03225G.
[122] R.K. Singh, T.H. Kim, K.D. Patel, J.C. Knowles, H.W. Kim, Biocompatible magnetite nanoparticles with varying silica-coating layer for use in biomedicine: physicochemical and magnetic properties, and cellular compatibility, J. Biomed. Mater. Res. – Part A (2012) 1734–1742, doi:http://dx.doi.org/10.1002/jbm.a.34140.
[123] A.V. Finn, M. Nakano, J. Narula, F.D. Kolodgie, R. Virmani, Concept of vulnerable/unstable plaque, Arterioscler. Thromb. Vasc. Biol. 30 (2010) 1282–1292, doi:http://dx.doi.org/10.1161/ATVBAHA.108.179739.
[124] J.D. Kratz, A. Chaddha, S. Bhattacharjee, S.N. Goonewardena, Atherosclerosis and nanotechnology: diagnostic and therapeutic applications, Cardiovasc. Drugs Ther. 30 (2016) 33–39, doi:http://dx.doi.org/10.1007/s10557-016-6649-2.
[125] J. Qin, C. Peng, B. Zhao, K. Ye, F. Yuan, Z. Peng, X. Yang, L. Huang, M. Jiang, Q. Zhao, G. Tang, X. Lu, Noninvasive detection of macrophages in atherosclerotic lesions by computed tomography enhanced with PEGylated gold nanoparticles, Int. J. Nanomed. 9 (2014) 5575–5590, doi:http://dx.doi.org/10.2147/IJN.S72819.
[126] P. Chhour, P.C. Naha, S.M. O'Neill, H.I. Litt, M.P. Reilly, V.A. Ferrari, D.P. Cormode, Labeling monocytes with gold nanoparticles to track their recruitment in atherosclerosis with computed tomography, Biomaterials 87 (2016) 93–103, doi:http://dx.doi.org/10.1016/j.biomaterials.2016.02.009.
[127] H. Orbay, H. Hong, Y. Zhang, W. Cai, Positron emission tomography imaging of atherosclerosis, Theranostics 3 (2013) 894–902, doi:http://dx.doi.org/10.7150/thno.5506.
[128] M. Nahrendorf, H. Zhang, S. Hembrador, P. Panizzi, D.E. Sosnovik, E. Aikawa, P. Libby, F.K. Swirski, R. Weissleder, Nanoparticle PET-CT imaging of macrophages in inflammatory atherosclerosis, Circulation 117 (2008) 379–387, doi:http://dx.doi.org/10.1161/CIRCULATIONAHA.107.741181.
[129] J.W. Seo, H. Baek, L.M. Mahakian, J. Kusunose, J. Hamzah, E. Ruoslahti, K.W. Ferrara, 64Cu-Labeled lyP-1-Dendrimer for PET-CT imaging of atherosclerotic plaque, Bioconjugate Chem. 25 (2014) 231–239, doi:http://dx.doi.org/10.1021/bc400347s.
[130] Y. Liu, M.J. Welch, Nanoparticles labeled with positron emitting nuclides: advantages, methods, and applications, Bioconjug. Chem. 23 (2012) 671–682, doi:http://dx.doi.org/10.1021/bc200264c.
[131] R. Weissleder, M. Nahrendorf, M.J. Pittet, Imaging macrophages with nanoparticles, Nat. Mater. 13 (2014) 125–138, doi:http://dx.doi.org/10.1038/nmat3780.
[132] I. Raynal, P. Prigent, S. Peyramaure, a Najid, C. Rebuzzi, C. Corot, Macrophage endocytosis of superparamagnetic iron oxide nanoparticles, Invest. Radiol. 39 (2004) 56–63, doi:http://dx.doi.org/10.1097/01.rli.0000101027.57021.28.

[133] K.J. Moore, F.J. Sheedy, E.A. Fisher, Macrophages in atherosclerosis: a dynamic balance, Nat. Rev. Immunol. 13 (2013) 709–721, doi:http://dx.doi.org/10.1038/nri3520.
[134] A. Usman, U. Sadat, A.J. Patterson, T.Y. Tang, K. Varty, J.R. Boyle, M.P. Armon, P. D. Hayes, M.J. Graves, J.H. Gillard, Use of ultrasmall superparamagnetic iron oxide particles for imaging carotid atherosclerosis, Nanomedicine (Lond) 10 (2015) 3077–3087, doi:http://dx.doi.org/10.2217/nnm.15.136.
[135] C. Tu, T.S.C. Ng, H.K. Sohi, H.A. Palko, A. House, R.E. Jacobs, A.Y. Louie, Receptor-targeted iron oxide nanoparticles for molecular MR imaging of inflamed atherosclerotic plaques, Biomaterials 32 (2011) 7209–7216, doi:http://dx.doi.org/10.1016/j.biomaterials.2011.06.026.
[136] D.G. You, G. Saravanakumar, S. Son, H.S. Han, R. Heo, K. Kim, I.C. Kwon, J.Y. Lee, J.H. Park, Dextran sulfate-coated superparamagnetic iron oxide nanoparticles as a contrast agent for atherosclerosis imaging, Carbohydr. Polym. 101 (2014) 1225–1233, doi:http://dx.doi.org/10.1016/j.carbpol.2013.10.068.
[137] G.Y. Lee, J.H. Kim, K.Y. Choi, H.Y. Yoon, K. Kim, I.C. Kwon, K. Choi, B.H. Lee, J.H. Park, I.S. Kim, Hyaluronic acid nanoparticles for active targeting atherosclerosis, Biomaterials 53 (2015) 341–348, doi:http://dx.doi.org/10.1016/j.biomaterials.2015.02.089.
[138] M. Kamat, K. El-Boubbou, D.C. Zhu, T. Lansdell, X. Lu, W. Li, X. Huang, Hyaluronic acid immobilized magnetic nanoparticles for active targeting and imaging of macrophages, Bioconjug. Chem. 21 (2010) 2128–2135, doi:http://dx.doi.org/10.1021/bc100354m.
[139] M.H. El-Dakdouki, K. El-Boubbou, M. Kamat, R. Huang, G.S. Abela, M. Kiupel, D.C. Zhu, X. Huang, CD44 targeting magnetic glyconanoparticles for atherosclerotic plaque imaging, Pharm. Res. 31 (2014) 1426–1437, doi:http://dx.doi.org/10.1007/s11095-013-1021-8.
[140] K. Tsuchiya, N. Nitta, A. Sonoda, H. Otani, M. Takahashi, K. Murata, M. Shiomi, Y. Tabata, S. Nohara, Atherosclerotic imaging using 4 types of superparamagnetic iron oxides: new possibilities for mannan-coated particles, Eur. J. Radiol. 82 (2013) 1919–1925, doi:http://dx.doi.org/10.1016/j.ejrad.2013.07.017.
[141] N.a. Jager, J. Westra, G.M. van Dam, N. Teteloshvili, R.a. Tio, J.-C. Breek, R.H.J.a. Slart, H. Boersma, P.S. Low, M. Bijl, C.J. Zeebregts, Targeted folate receptor fluorescence imaging as a measure of inflammation to estimate vulnerability within human atherosclerotic carotid plaque, J. Nucl. Med. 53 (2012) 1222–1229, doi:http://dx.doi.org/10.2967/jnumed.111.099671.
[142] P. Periyathambi, T. Sastry, S. Anandasadagopan, K. Manickavasagam, Macrophages mediated diagnosis of rheumatoid arthritis using fibrin based magnetic nanoparticles as MRI contrast agents, Biochim. Biophys. Acta 1861 (2017) 2992–3001.
[143] S. Blankenberg, S. Barbaux, L. Tiret, Adhesion molecules and atherosclerosis, Atherosclerosis 170 (2003) 191–203, doi:http://dx.doi.org/10.1016/S0021-9150(03)00097-2.
[144] K.A. Kelly, J.R. Allport, A. Tsourkas, V.R. Shinde-Patil, L. Josephson, R. Weissleder, Detection of vascular adhesion molecule-1 expression using a novel multimodal nanoparticle, Circ. Res. 96 (2005) 327–336, doi:http://dx.doi.org/10.1161/01.RES.0000155722.17881.dd.
[145] M. Michalska, L. MacHtoub, H.D. Manthey, E. Bauer, V. Herold, G. Krohne, G. Lykowsky, M. Hildenbrand, T. Kampf, P. Jakob, A. Zernecke, W.R. Bauer, Visualization of vascular inflammation in the atherosclerotic mouse by ultrasmall superparamagnetic iron oxide vascular cell adhesion molecule-1-specific nanoparticles, Arterioscler. Thromb. Vasc. Biol. 32 (2012) 2350–2357, doi:http://dx.doi.org/10.1161/ATVBAHA.112.255224.
[146] M.J. Jacobin-Valat, K. Deramchia, S. Mornet, C.E. Hagemeyer, S. Bonetto, R. Robert, M. Biran, P. Massot, S. Miraux, S. Sanchez, A.K. Bouzier-Sore, J.M. Franconi, E. Duguet, G. Clofent-Sanchez, MRI of inducible P-selectin expression in human activated platelets involved in the early stages of atherosclerosis, NMR Biomed. 24 (2011) 413–424, doi:http://dx.doi.org/10.1002/nbm.1606.
[147] M.J. Jacobin-Valat, J. Laroche-Traineau, M. Lariviére, S. Mornet, S. Sanchez, M. Biran, C. Lebaron, J. Boudon, S. Lacomme, M. Cérutti, G. Clofent-Sanchez, Nanoparticles functionalised with an anti-platelet human antibody for in vivo detection of atherosclerotic plaque by magnetic resonance imaging, Nanomed. Nanotechnol. Biol. Med. 11 (2015) 927–937, doi:http://dx.doi.org/10.1016/j.nano.2014.12.006.
[148] L. Bachelet-Violette, A.K.A. Silva, M. Maire, A. Michel, O. Brinza, P. Ou, V. Ollivier, A. Nicoletti, C. Wilhelm, D. Letourneur, C. Ménager, F. Chaubet, Strong and specific interaction of ultra small superparamagnetic iron oxide nanoparticles and human activated platelets mediated by fucoidan coating, RSC Adv. 4 (2014) 4864, doi:http://dx.doi.org/10.1039/c3ra46757k.
[149] M. Suzuki, L. Bachelet-Violette, F. Rouzet, A. Beilvert, G. Autret, M. Maire, C. Menager, L. Louedec, C. Choqueux, P. Sabboural, O. Haddad, C. Chauvierre, F. Chaubet, J.-B. Michel, J.-M. Serfaty, D. Letourneur, Ultrasmall superparamagnetic iron oxide nanoparticles coated with fucoidan for molecular MRI of intraluminal thrombus, Nanomedicine 10 (2015) 73–87, doi:http://dx.doi.org/10.2217/nnm.14.51.
[150] S. Wagner, J. Schnorr, A. Ludwig, V. Stangl, M. Ebert, B. Hamm, M. Taupitz, Contrast-enhanced MR imaging of atherosclerosis using citrate-coated superparamagnetic iron oxide nanoparticles: calcifying microvesicles as imaging target for plaque characterization, Int. J. Nanomed. 8 (2013) 767–779, doi:http://dx.doi.org/10.2147/IJN.S38702.
[151] C. Scharlach, H. Kratz, F. Wiekhorst, C. Warmuth, J. Schnorr, G. Genter, M. Ebert, S. Mueller, E. Schellenberger, Synthesis of acid-stabilized iron oxide nanoparticles and comparison for targeting atherosclerotic plaques: evaluation by MRI, quantitative MPS, and TEM alternative to ambiguous Prussian blue iron staining, Nanomed. Nanotechnol. Biol. Med. 11 (2015) 1–11, doi:http://dx.doi.org/10.1016/j.nano.2015.01.002.
[152] T.Y. Tang, K.H. Muller, M.J. Graves, Z.Y. Li, S.R. Walsh, V. Young, U. Sadat, S.P.S. Howarth, J.H. Gillard, Iron oxide particles for atheroma imaging, Arterioscler. Thromb. Vasc. Biol. 29 (2009) 1001–1008, doi:http://dx.doi.org/10.1161/ATVBAHA.108.165514.
[153] M.E. Kooi, V.C. Cappendijk, Cleutjens K.B.J.M, A.G.H. Kessels, Kitslaar P.J.E.H. M, M. Borgers, P.M. Frederik, Daemen M.J.A.P, J.M.A. Van Engelshoven, Accumulation of ultrasmall superparamagnetic particles of iron oxide in human atherosclerotic plaques can be detected by in vivo magnetic resonance imaging, Circulation 107 (2003) 2453–2458, doi:http://dx.doi.org/10.1161/01.CIR.0000068315.98705. CC.
[154] R.A. Trivedi, J.M. U-King-Im, M.J. Graves, J.J. Cross, J. Horsley, M.J. Goddard, J.N. Skepper, G. Quartey, E. Warburton, I. Joubert, L. Wang, P.J. Kirkpatrick, J. Brown, J.H. Gillard, In vivo detection of macrophages in human carotid atheroma: temporal dependence of ultrasmall superparamagnetic particles of iron oxide-enhanced MRI, Stroke 35 (2004) 1631–1635, doi:http://dx.doi.org/10.1161/01.STR.0000131268.50418.b7.
[155] R.A. Trivedi, C. Mallawarachi, J.M. U-King-Im, M.J. Graves, J. Horsley, M.J. Goddard, A. Brown, L. Wang, P.J. Kirkpatrick, J. Brown, J.H. Gillard, Identifying inflamed carotid plaques using in vivo USPIO-enhanced MR imaging to label plaque macrophages, Arterioscler. Thromb. Vasc. Biol. 26 (2006) 1601–1606, doi:http://dx.doi.org/10.1161/01.ATV.0000222920.59760.df.
[156] A. Yilmaz, S. Rösch, H. Yildiz, S. Klumpp, U. Sechtem, First multiparametric cardiovascular magnetic resonance study using ultrasmall superparamagnetic iron oxide nanoparticles in a patient with acute myocardial infarction: new vistas for the clinical application of ultrasmall superparamagnetic iron oxide, Circulation 126 (2012) 1932–1934, doi:http://dx.doi.org/10.1161/CIRCULATIONAHA.112.108167.
[157] S.R. Alam, A.S.V. Shah, J. Richards, N.N. Lang, G. Barnes, N. Joshi, T. MacGillivray, G. McKillop, S. Mirsadraee, J. Payne, K.A.A. Fox, P. Henriksen, D.E. Newby, S.I.K. Semple, Ultrasmall superparamagnetic particles of iron oxide in patients with acute myocardial infarction early clinical experience, Circ. Cardiovasc. Imaging 5 (2012) 559–565, doi:http://dx.doi.org/10.1161/CIRCIMAGING.112.974907.
[158] B.R. Jarrett, C. Correa, K.L. Ma, A.Y. Louie, In vivo mapping of vascular inflammation using multimodal imaging, PLoS One 5 (2010) 2–9, doi:http://dx.doi.org/10.1371/journal.pone.0013254.
[159] C. Tu, T.S.C. Ng, R.E. Jacobs, A.Y. Louie, Multimodality PET/MRI agents targeted to activated macrophages, J. Biol. Inorg. Chem. 19 (2014) 247–258, doi:http://dx.doi.org/10.1007/s00775-013-1054-9.
[160] D. Cheng, X. Li, C. Zhang, H. Tan, C. Wang, L. Pang, H. Shi, Detection of vulnerable atherosclerosis plaques with a dual-modal single-photon-emission computed tomography/magnetic resonance imaging probe targeting apoptotic macrophages, ACS Appl. Mater. Interfaces 7 (2015) 2847–2855, doi:http://dx.doi.org/10.1021/am508118x.
[161] F.A. Jaffer, M. Nahrendorf, D. Sosnovik, K.A. Kelly, E. Aikawa, R. Weissleder, Cellular imaging of inflammation in atherosclerosis using magnetofluorescent nanomaterials, Mol. Imaging 5 (2006) 85–92, doi:http://dx.doi.org/10.2310/7290.2006.00009.
[162] Y. Wang, J. Chen, B. Yang, H. Qiao, L. Gao, T. Su, S. Ma, X. Zhang, X. Li, G. Liu, J. Cao, X. Chen, Y. Chen, F. Cao, In vivo MR and fluorescence dual-modality imaging of atherosclerosis characteristics in mice using profilin-1 targeted magnetic nanoparticles, Theranostics 6 (2016) 272–286, doi:http://dx.doi.org/10.7150/thno.13350.
[163] H. Qiao, Y. Wang, R. Zhang, Q. Gao, X. Liang, L. Gao, Z. Jiang, R. Qiao, D. Han, Y. Zhang, Y. Qiu, J. Tian, M. Gao, F. Cao, MRI/optical dual-modality imaging of vulnerable atherosclerotic plaque with an osteopontin-targeted probe based on Fe3O4 nanoparticles, Biomaterials 112 (2017) 336–345, doi:http://dx.doi.org/10.1016/j.biomaterials.2016.10.011.
[164] Y. Song, Z. Huang, J. Xu, D. Ren, Y. Wang, X. Zheng, Y. Shen, L. Wang, H. Gao, J. Hou, Z. Pang, J. Qian, J. Ge, Multimodal SPION-CREKA peptide based agents for molecular imaging of microthrombus in a rat myocardial ischemia-reperfusion model, Biomaterials 35 (2014) 2961–2970, doi:http://dx.doi.org/10.1016/j.biomaterials.2013.12.038.
[165] N. Lee, H.R. Cho, M.H. Oh, S.H. Lee, K. Kim, B.H. Kim, K. Shin, T. Ahn, J.W. Choi, Y. Kim, S.H. Choi, T. Hyeon, Multifunctional Fe 3 O 4/TaO, J. Am. Chem. Soc. 134 (2012) 10309–10312, doi:http://dx.doi.org/10.1021/ja3016582.
[166] S. Narayanan, B.N. Sathy, U. Mony, M. Koyakutty, S.V. Nair, D. Menon, Biocompatible magnetite/gold nanohybrid contrast agents via green chemistry for MRI and CT bioimaging, ACS Appl. Mater. Interfaces 4 (2012) 251–260, doi:http://dx.doi.org/10.1021/am201311c.
[167] J.K.H. Liu, The history of monoclonal antibody development–progress, remaining challenges and future innovations, Ann. Med. Surg. 3 (2014) 113–116.
[168] K. Oumzil, M.A. Ramin, C. Lorenzato, A. Hémadou, J. Laroche, M.J. Jacobin-Valat, S. Mornet, C.E. Roy, T. Kauss, K. Gaudin, G. Clofent-Sanchez, P. Barthélémy, Solid lipid nanoparticles for image-guided therapy of atherosclerosis, Bioconjug. Chem. 27 (2016) 569–575, doi:http://dx.doi.org/10.1021/acs.bioconjchem.5b00590.
[169] T.F. Lüscher, U. Landmesser, A. Von Eckardstein, A.M. Fogelman, High-density lipoprotein: vascular protective effects, dysfunction, and potential as therapeutic target, Circ. Res. 114 (2014) 171–182, doi:http://dx.doi.org/10.1161/CIRCRESAHA.114.300935.
[170] V. Nandwana, S.-R. Ryoo, S. Kanthala, K.M. McMahon, J.S. Rink, Y. Li, S.S. Venkatraman, C.S. Thaxton, V.P. Dravid, High-density lipoprotein-like

magnetic nanostructures (HDL-MNS): theranostic agents for cardiovascular disease, Chem. Mater. 29 (2017) 2276–2282, doi:http://dx.doi.org/10.1021/acs.chemmater.6b05357.
[171] F. Nensa, K. Beiderwellen, P. Heusch, A. Wetter, Clinical applications of PET/MRI: current status and future perspectives, Diagn. Interv Radiol. 20 (2014) 438–447, doi:http://dx.doi.org/10.5152/dir.2014.14008.
[172] F.A. Jaffer, J.W. Verjans, Molecular imaging of atherosclerosis: clinical state-of-the-art, Heart 100 (2013) 1469–1477, doi:http://dx.doi.org/10.1136/heartjnl-2011-301370.

Glossary

CT: Computed tomography
DMSA: Dimercaptosuccinic acid
DOTA: 1,4,7,10 tetraazacyclododecane-1,4,7,10-teraacetic acid
DTPA: Diethylenetriamine penta-acetic acid
FICT: Fluorescein isothiocyanate
FMT: Fluorescence molecular tomography
GAGs: Glycosaminoglycans
GBCAs: Gadolinium based contrast agents
HA: Hyaluronic acid
ICAM: Intercellular adhesion molecules
MRI: Magnetic resonance imaging
MNP: Nanoparticles based on magnetic iron oxide
MPS: Mononuclear phagocytic system.
NFS: Nephrogenic systemic fibrosis
PAT: Photoacoustic tomography
PEG: Polyethylene glycol
PET: Positron emission tomography
SDIO: Dextran sulfate coated-MNPs
SPET: Single-photon emission computed tomography
SPIONs: Super-paramagnetic iron oxide nanoparticles
SR-A: Scavenger receptor
USPIONs: Ultra-small super-paramagnetic iron oxide nanoparticles
VCAM-1: Vascular cell adhesion molecules
VSMCs: Vascular smooth muscle cells